AD-A210 592

The Robotics Institute

Carnegie-Mellon University

REPORT DOCUMENTATION PAGE

1a. REPORT SECURITY CLASSIFICATION Unclassified		1b. RESTRICTIVE MARKINGS
2a. SECURITY CLASSIFICATION AUTHORITY		3 DISTRIBUTION / AVAILABILITY OF REPORT Approved for public release; distribution unlimited
2b. DECLASSIFICATION / DOWNGRADING SCHEDULE		

4. PERFORMING ORGANIZATION REPORT NUMBER(S) CMU-RI-TR-89-7	5. MONITORING ORGANIZATION REPORT NUMBER(S)

6a. NAME OF PERFORMING ORGANIZATION The Robotics Institute Carnegie Mellon University	6b OFFICE SYMBOL (If applicable)	7a. NAME OF MONITORING ORGANIZATION
6c. ADDRESS (City, State, and ZIP Code) Pittsburgh, PA 15213		7b. ADDRESS (City, State, and ZIP Code)

8a. NAME OF FUNDING / SPONSORING ORGANIZATION DARPA	8b. OFFICE SYMBOL (If applicable)	9. PROCUREMENT INSTRUMENT IDENTIFICATION NUMBER F33615-87-C-1499

8c. ADDRESS (City, State, and ZIP Code)	10. SOURCE OF FUNDING NUMBERS			
	PROGRAM ELEMENT NO.	PROJECT NO.	TASK NO.	WORK UNIT ACCESSION NO.

11. TITLE (Include Security Classification)
Surface Reflection: Physical and Geometrical Perspectives

12. PERSONAL AUTHOR(S)
Shree K. Nayar, Katsushi Ikeuchi, and Takeo Kanade

13a. TYPE OF REPORT Technical	13b. TIME COVERED FROM _____ TO _____	14. DATE OF REPORT (Year, Month, Day) March 1989	15. PAGE COUNT 53

16. SUPPLEMENTARY NOTATION
This work was supported by the Westinghouse Electric Corporation

17.	COSATI CODES		18. SUBJECT TERMS (Continue on reverse if necessary and identify by block number)
FIELD	GROUP	SUB-GROUP	machine vision; reflectance models; physical; geometrical optics; surface imperfections;

19. ABSTRACT (Continue on reverse if necessary and identify by block number)

Machine vision can greatly benefit from the development of accurate reflectance models. There are two approaches to the study of reflection: physical and geometrical optics. While geometrical models may be construed as mere approximations to physical models, they possess simpler mathematical forms that often render them more usable than physical models. However, geometrical models are applicable only when the wavelength of incident light is small compared to the dimensions of the surface imperfections. Therefore, it is incorrect to use these models to interpret or predict reflections from smooth surfaces, and only physical models are capable of describing the underlying reflection mechanism.

This paper is directed towards unifying physical and geometrical approaches to describe reflection from surfaces that may vary from smooth to rough. More specifically, we consider the Beckmann-Spizzichino (physical optics) model and the Torrance-Sparrow (geometrical optics) model. We have chosen these two models in particular as they have been reported to fit experimental data very well. Each model is described in detail, and the conditions that

20. DISTRIBUTION / AVAILABILITY OF ABSTRACT ☒ UNCLASSIFIED/UNLIMITED ☐ SAME AS RPT. ☐ DTIC USERS	21. ABSTRACT SECURITY CLASSIFICATION Unclassified
22a. NAME OF RESPONSIBLE INDIVIDUAL	22b. TELEPHONE (Include Area Code) 22c. OFFICE SYMBOL

(19 cont'd.)

determine the validity of the model are clearly stated. From studying the behaviors of both models, we propose a model comprising three reflection components: the diffuse lobe, the specular lobe, and the specular spike. The dependencies of the three components on the surface roughness and the angles of incidence and reflection are analyzed in detail.

Surface Reflection:
Physical and Geometrical Perspectives

Shree K. Nayar, Katsushi Ikeuchi, and Takeo Kanade

CMU-RI-TR-89-7

The Robotics Institute
Carnegie Mellon University
Pittsburgh, Pennsylvania 15213

March 1989

Contents

Abstract

Machine vision can greatly benefit from the development of accurate reflectance models. There are two approaches to the study of reflection: physical and geometrical optics. While geometrical models may be construed as mere approximations to physical models, they possess simpler mathematical forms that often render them more usable than physical models. However, geometrical models are applicable only when the wavelength of incident light is small compared to the dimensions of the surface imperfections. Therefore, it is incorrect to use these models to interpret or predict reflections from smooth surfaces, and only physical models are capable of describing the underlying reflection mechanism.

This paper is directed towards unifying physical and geometrical approaches to describe reflection from surfaces that may vary from smooth to rough. More specifically, we consider the Beckmann-Spizzichino (physical optics) model and the Torrance-Sparrow (geometrical optics) model. We have chosen these two models in particular as they have been reported to fit experimental data very well. Each model is described in detail, and the conditions that determine the validity of the model are clearly stated. From studying the behaviors of both models, we propose a model comprising three reflection components: the diffuse lobe, the specular lobe, and the specular spike. The dependencies of the three components on the surface roughness and the angles of incidence and reflection are analyzed in detail.

Accession For	
NTIS GRA&I	☑
DTIC TAB	☐
Unannounced	☐
Justification	
By	
Distribution/	
Availability Codes	
Dist	Avail and/or Special
A-1	

ii

1 Introduction

Most machine vision problems involve the analysis of images resulting from the reflection of light. The apparent brightness of a point depends on its ability to reflect incident light in the direction of the sensor: what is commonly known as its reflectance properties. Therefore, the prediction or interpretation of image intensities requires a sound understanding of the various mechanisms involved in the reflection process. While shape extraction and object recognition methods are being refined, it is also essential for the vision community to research and utilize more sophisticated reflectance models. Once a "general" reflectance model is made available, we are free to make reflectance assumptions that are reasonable for the vision application at hand. The resulting more specific model may then be used to develop efficient perception techniques.

Various reflectance models have been used in the areas of machine vision and graphics. Horn [8] used the Lambertian diffuse reflectance model and the double-delta specular reflectance model to develop shape-from-shading algorithms for machine vision. Horn [7] has also provided an excellent review of some of the early models used in graphics for hill shading. Phong [19] proposed a parametrized continuous function to represent specular reflectance, and used the model to produce computer-synthesized images of objects. Woodham [32] used the Lambertian model to determine object shape by means of photometric stereo. Ikeuchi [12] used the double-delta specular model to determine the shape of specular surfaces by photometric stereo. Pentland [18] developed a local shape-from-shading algorithm that assumes Lambertian reflectance. Coleman and Jain [4] proposed the four-source photometric stereo, which discards specular reflections and uses the diffuse reflections and the Lambertian model to determine shape information. Sanderson, Weiss, and Nayar [24] have used the double-delta specular model to determine the shape of specular surfaces by means of the structured highlight technique. Recently, Nayar, Ikeuchi, and Kanade [16] have developed the photometric sampling method that uses a hybrid reflectance model, comprised of both Lambertian and specular models, to extract the shape and reflectance of Lambertian, specular, and hybrid surfaces.

The above applications have proven that the Lambertian model does reasonably well in describing diffuse reflections. Moreover, its simple functional form has made it a popular reflectance model in the vision research community. On the other hand, the specular models used above perform well only when the object surface is very smooth, in which case, most of the reflected light is concentrated around the specular direction. Specular reflection from rough surfaces, however, requires careful examination, and its dependence on the imaging and illumination geometry can only be obtained by a formal treatment of optics. There are two different approaches to optics, and thus two different approaches to the study of reflection. The physical optics approach uses electromagnetic wave theory to study the reflection of incident light. The geometrical optics approach, on the other hand, uses the

short wavelength of light to simplify the reflection problem. Hence, geometrical models may be viewed as approximations to physical models.

The Beckmann-Spizzichino physical optics model and the Torrance-Sparrow geometrical optics model have recently attracted considerable attention. Both models have been developed to describe specular reflection mechanisms, and both have been found to fit experimental data quite well [11] [30]. Owing to its simpler mathematical form, the Torrance-Sparrow model is more popular than the Beckmann-Spizzichino model, and has been used in the areas of computer vision and graphics. Healey and Binford [6] have used the Torrance-Sparrow model to determine local shape from specular reflections. Wolff [31] has used the model to develop spectral and polarization stereo methods. Cook and Torrance [5] have modified the model and used it to render images of objects. Tagare and Figueiredo [29] have discussed both the Beckmann-Spizzichino and the Torrance-Sparrow models in their survey of various reflection mechanisms.

When applying physical and geometrical models, it is important to satisfy the conditions that determine the validity of the models. This requires an understanding of the restrictions imposed by the assumptions made while developing the models. Most of these assumptions are related to the microscopic shape and physical properties of the reflecting surface. In this paper, we seek answers to the following questions: How are surface shapes modeled, and when is a surface rough? How are physical optics and geometrical optics models developed? Under what conditions are the Beckmann-Spizzichino and the Torrance-Sparrow models valid? How do the reflectance curves predicted by the two models compare with one another, and how are the surface roughness parameters of the two models related to each other? What are the primary components of surface reflection, and which model should be used to represent each of the primary components? How are the reflection components dependent on the surface roughness, and on the angles of incidence and reflection?

In section 2 of this paper, we define radiometric concepts that are useful in the analysis of surface reflection. In section 3, we look at different approaches to modeling surface profiles. In section 4, we highlight the main steps that are involved in the derivation of the Beckmann-Spizzichino and Torrance-Sparrow models, and clearly state the assumptions made in the process of their development. On the basis of the reflectance curves predicted by the two models, we propose a reflectance model that has three primary components: the *diffuse lobe*, the *specular lobe*, and the *specular spike*. In section 5, we study these reflectance components in detail.

2 Radiometric Definitions

In this section, we present definitions of radiometric terms that are useful in the study of surface reflection. Detailed derivations and descriptions of these terms are given by
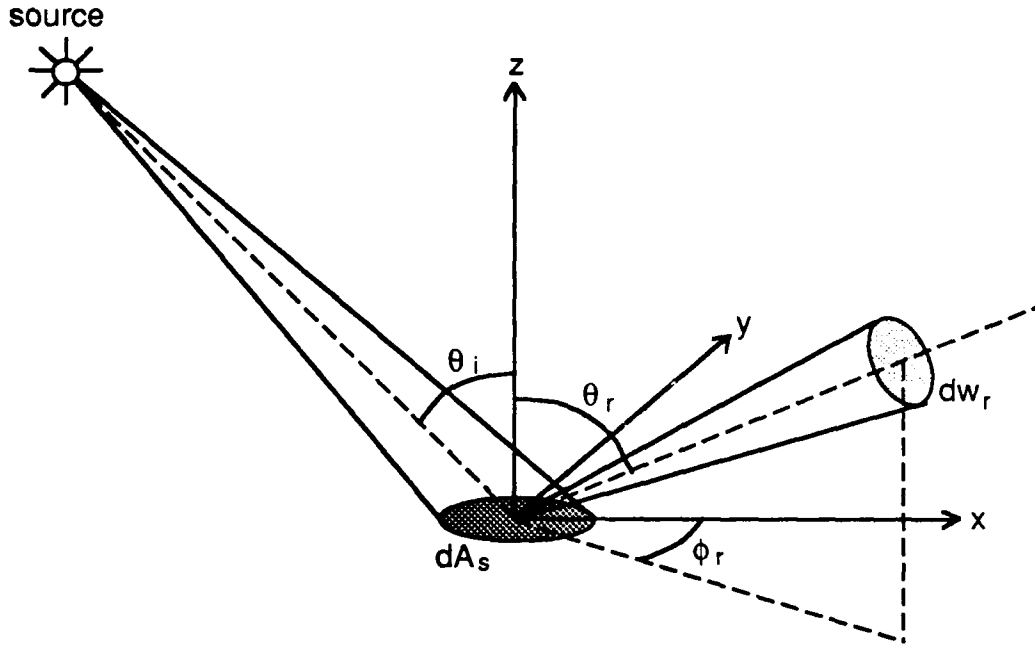
Figure 1: Basic geometry needed to define radiometric terms.

Nicodemus et al. [17]. As shown in Figure 1, all directions are represented by the zenith angle θ and the azimuth angle ϕ. The light source is assumed to lie in the x-z plane and is therefore uniquely determined by its zenith angle θ_i. The monochromatic flux $d\Phi_i$ is incident on the surface area dA_s from the direction θ_i, and a fraction of it, $d^2\Phi_r$, is reflected in the direction (θ_r, ϕ_r). The *irradiance* I_s[1] of the surface is defined as the incident flux density:

$$I_s = \frac{d\Phi_i}{dA_s} \,.$$ (1)

The *radiance* L_r of the surface is defined as the flux emitted per unit fore-shortened area per unit solid angle. The surface radiance in the direction (θ_r, ϕ_r) is defined as:

$$L_r = \frac{d^2\Phi_r}{dA_s \cos\theta_r \, d\omega_r} \,.$$ (2)

The BRDF (*Bi-Directional Reflectance Distribution Function*) f_r of a surface is a measure of how bright the surface appears when viewed from a given direction, when it is illuminated

---

[1] Irradiance is usually [8] denoted by the symbol E. In the following sections, we will be using E to denote the electric field, and therefore we will denote irradiance by I to avoid confusion.

3

from another given direction. The BRDF is defined as:

$$f_r = \frac{L_r}{I_s} .$$

(3)

In the following sections of this paper, we will frequently use the above radiometric definitions.

3 Surface Model

The manner in which light is reflected by a surface is dependent on, among other factors, the microscopic shape characteristics of the surface. A smooth surface, for instance, may reflect incident light in a single direction, while a rough surface will tend to scatter light in various directions, maybe more in some directions than others. To be able to accurately predict the reflection of incident light, we must have prior knowledge of the microscopic surface irregularities; in other words, we need a model of the surface. All possible surface models may be divided into two broad categories: surfaces with exactly known profiles and surfaces with random irregularities. An exact profile may be determined by measuring the height at each point on the surface by means of a sensor such as the *stylus profilometer*. This method, however, is quite cumbersome and also inapplicable in many practical situations. Hence, it is often convenient to model a surface as a random process, where it is described by a statistical distribution of either its height above a certain mean level, or its slope with respect to its mean (macroscopic) slope. In this section, we discuss these two approaches to surface modeling in greater detail and explain how surface roughness is pertinent to the study of reflection.

3.1 Height Distribution Model

The height coordinate h of the surface may be expressed as a random function of the coordinates x and y, as shown in Figure 2. The shape of the surface is then determined by the probability distribution of h. For instance, let h be normally distributed, with mean value $<h> = 0$, and standard deviation σ_h. Then, the distribution of h is given by:

$$p_h(h) = \frac{1}{\sqrt{2\pi}\sigma_h} e^{-\frac{h^2}{2\sigma_h^2}} .$$

(4)

The standard deviation σ_h is also the root-mean-square of h and represents the *roughness* of the surface. The surface *is not uniquely described by the statistical distribution of h*, however, as it does not tell us anything about the distances between the hills and valleys of
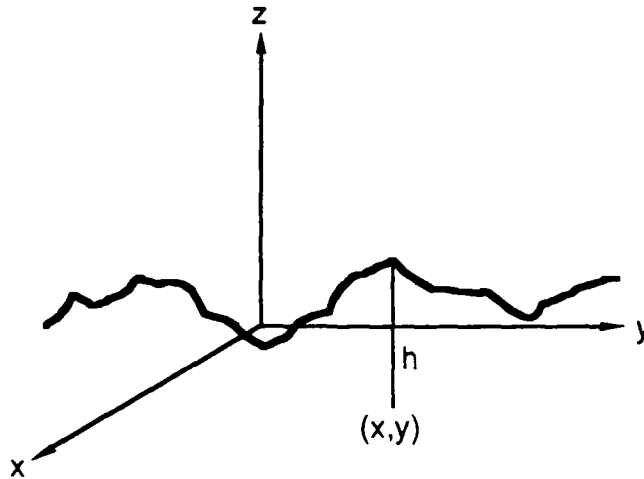
4

Figure 2: Surface height as a random function of the spatial coordinates.

the surface. In Figure 3, both surfaces (a) and (b) have the same height distribution function, i.e. the same mean value and standard deviation. In appearance, however, the two surfaces do not strongly resemble each other. In order to strengthen our surface model, we use an autocorrelation coefficient $C(\tau)$ that determines the correlation (or lack of independence) between the random values assumed by the height h at two surface points (x_1, y_1) and (x_2, y_2), separated by a distance τ. We describe the autocorrelation coefficient by the fairly general function:

$$C(\tau) = e^{-\frac{\tau^2}{T^2}} \, , \tag{5}$$

where T is the *correlation distance*, for which $C(\tau)$ drops to the value e^{-1}. We see that the surfaces (a) and (b) shown in Figure 3 have small and large correlation distances, respectively. By varying the parameters σ_h and T of our surface model, we can generate surfaces that match in appearance almost any rough surface met in practice. Moreover, if we are dissatisfied with the performance of the model, we can always use another height distribution function and/or another autocorrelation function than the ones given above.

3.2 Slope Distribution Model

It is sometimes convenient to think of a surface as a collection of planar micro-facets, as illustrated in Figure 4. A large set of micro-facets constitutes an infinitesimal surface patch that has a mean surface orientation **n**. Each micro-facet, however, has its own orientation, which may deviate from the mean surface orientation by an angle α. We will use the
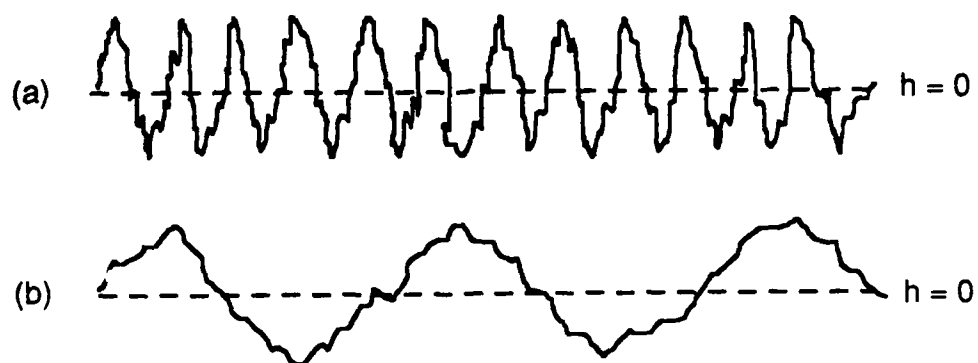
5

Figure 3: Random surfaces with (a) small, (b) large correlation distances.
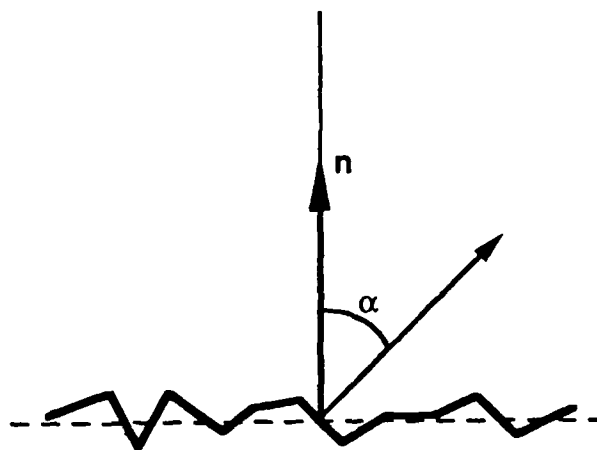

Figure 4: Surface modeled as a collection of planar micro-facets.

parameter α to represent the slope of individual facets. Surfaces can be modeled by a statistical distribution of the micro-facet slopes. If the surface is isotropic, the probability distribution of the micro-facet slopes can be assumed to be rotationally symmetric with respect to the mean surface normal n. Therefore, facet slopes may be described by a one-dimensional probability distribution function. For example, the surface may be modeled by assuming a normal distribution for the facet slope α, with mean value $<\alpha> = 0$ and standard deviation σ_α:

$$p_\alpha(\alpha) = \frac{1}{\sqrt{2\pi}\sigma_\alpha} e^{-\frac{\alpha^2}{2\sigma_\alpha^2}} . \tag{6}$$

The surface model in this case is determined by a single parameter, namely, σ_α, unlike the height distribution model, which requires two parameters. Larger values of σ_α may be used to model rougher surfaces. While the importance of an autocorrelation coefficient was shown for the height model, the concept of slope correlation is more difficult to interpret and, therefore, is not of much use in the generation of surfaces. The advantages of using a single parameter come with the cost of a weaker model when compared to the height model. Given a probability distribution function for α, it is difficult to visualize the shape of the surface and to estimate the root-mean-square height of the surface. However, the slope distribution model is popular in the analysis of surface reflection, as the scattering of light rays has been found to be dependent on the local slope of the surface and not the local height of the surface. For this reason, the slope model, though relatively ambiguous, is more directly applicable to the problem of surface reflection. Shortly, we will see how both height and slope models are used to develop surface reflection models.

3.3   What is a Rough Surface?

One would expect humans to respond to this question with a variety of answers. We seem to have a rather loose definition of the term "roughness." A surface that appears to be rough from a short distance may appear to be smooth from far away. In some cases, by changing the direction of illumination, surface imperfections can be made less visible and a rough surface can be made to appear smooth. If the observer is unable to discern from its appearance how rough the surface is, he or she is inclined to feel the surface and make a judgment on the basis of the resulting sensation.

In contrast to the human definition of roughness, surface reflection theories offer a stronger definition: one that relates surface irregularities to the wavelength of incident light and the angle of incidence. For incident light of a given wavelength, the roughness of a surface may be estimated by studying the manner in which the surface scatters light in different directions. If the surface irregularities are small compared to the wavelength of incident light, a large fraction of the incident light will be reflected *specularly* in a single

direction. On the other hand, if surface irregularities are large compared to the wavelength, the surface will scatter the incident light in various directions. Conversely, the same surface can be made to appear smooth or rough by varying the wavelength of incident light; or for the same wavelength it can be made to appear smooth or rough by varying the angle of incidence.

Raleigh suggested a way of relating surface roughness to wavelength and angle of incidence, and established a simple criterion for classifying surfaces as smooth or rough. Consider rays 1 and 2 in Figure 5, incident at an angle β on a surface with irregularities of height H. Since the two rays strike the surface at locally smooth patches, both rays are specularly reflected. The rays originate from a source plane that is perpendicular to the rays, and they are received by a detector plane that is perpendicular to the reflected rays. We
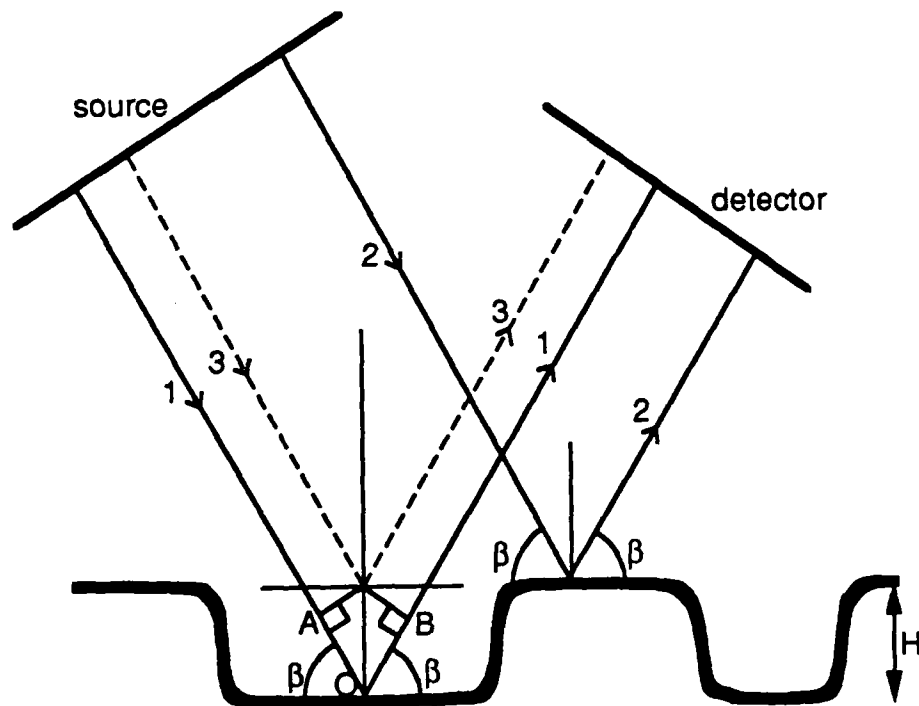

Figure 5: Analyzing surface roughness from the view point of reflection.

are interested in finding the difference between the paths traveled by the two rays. Using basic geometry it can be shown that ray 2 and the imaginary ray 3 travel the same distance. Therefore, the path difference Δd between rays 1 and 2 is equal to the path difference AOB

between rays 1 and 3, and is determined as:

$$\Delta d = 2H sin\beta .$$
(7)

If λ is the wavelength of the incident rays, the phase difference between the rays received by the detector may be determined from the path difference as:

$$\Delta\Omega = \frac{4\pi H}{\lambda} sin\beta .$$
(8)

When $\Delta\Omega$ is very small, the two rays received by the detector will be almost in phase with each other, and the received energy will be nearly equal to the sum of the energies carried by the two rays. In this case, the surface reflects light specularly. However, as the phase difference approaches π, the the two rays will be in phase opposition and will tend to cancel the effects of each other. In fact, at $\Delta\Omega = \pi$ no energy will flow in the direction of the detector. The incident energy is thus redistributed in other directions, and the law of conservation of energy is preserved. Hence, the extreme cases are: $\Delta\Omega = 0$, when the surface reflects light specularly and is thus smooth; and $\Delta\Omega = \pi$, when the surface scatters light and is rough. We can thus classify surfaces as smooth and rough by picking an arbitrary threshold between $\Delta\Omega = 0$ and $\Delta\Omega = \pi$. By selecting a threshold value of $\pi/2$ we have the *Raleigh criterion* that states that a surface is considered to be rough when:

$$H > \frac{\lambda}{8 sin\beta} .$$
(9)

This is, of course, a rather simple approach to determining the roughness of a surface. Some papers that discuss the height distribution model have defined a rough surface as one whose root-mean-square height is much greater than the wavelength of incident light, i.e. $\sigma_h \gg \lambda$. More sophisticated criteria have been developed since the Raleigh criterion was first proposed. We will not pursue these criteria here but direct the interested reader to [1] for a more detailed treatment. In fact, we have described the Raleigh criterion only to bring forth the concept of roughness and to emphasize its significance in the study of surface reflection.

4 Reflection Model

When light is incident on a boundary interface between two different media, it is reflected according to well-known laws. There are two different approaches to optics and, consequently, two different approaches to the study of reflection. *Physical* or *wave* optics is based directly on electromagnetic wave theory and uses Maxwell's equations to study the propagation of light. *Geometrical* or *ray* optics, on the other hand, uses the short wavelength of light to simplify many of the light propagation problems. Geometrical optics is generally able to

9

explain the gross behavior of light when the wavelength is small compared to the pertinent physical dimensions of the system (in our case, the surface imperfections).

In this section, we study surface reflection from the perspective of physical and geometrical optics. More specifically, we discuss a physical optics reflection model, namely, the Beckmann-Spizzichino model, and a geometrical optics reflection model, namely, the Torrance-Sparrow model. We highlight the main steps that are involved in the derivation of both models and clearly state the assumptions made in the process of their development. The derivations will draw on the surface modeling approaches discussed in the previous section. Later, the two models are compared by plotting the predicted reflectance as functions of viewer and source directions.

4.1 Physical Optics Model

Light is an electromagnetic phenomenon. Therefore, in a strict sense, optics should be studied as a branch of electrodynamics. Optics is usually treated as a separate field because it was studied long before its electromagnetic character was realized. Before we address the *scattering* of incident light waves by smooth and rough surfaces, we feel that a very brief introduction to electromagnetic waves is in order.

4.1.1 Electromagnetic Waves

In the atomic theory of matter, electromagnetic effects are considered to arise from the forces exerted on each other by elementary charged particles. The elementary positive and negative particles are the proton and electron, respectively. Consider two charged particles placed in the vicinity of each other. Due to their respective charges, the particles will exert a force on each other. If the particles are at rest, they will experience a constant electrostatic force resulting from the *electric field* generated by them. However, if the particles have different relative velocities with respect to a common frame of reference, the force acting between them will differ from the electrostatic force. This statement can be verified by simple experiments [2]. The discrepancy between the forces experienced when the particles are at rest and when they are in relative motion suggests the presence of another field, namely, the *magnetic field*, in addition to the electric field. In fact, Maxwell's equations may be interpreted as a mathematical formalization of the following physical phenomenon: associated with a time-varying electric field is a magnetic field. Therefore, the forces experienced by a moving charge can be conveniently represented by means of electromagnetic field vectors: the *electric field intensity* E and the *magnetic field intensity* H. Conversely, an electromagnetic field may be generated by applying forces and physically moving charges in some region of space. The electromagnetic field does not require a medium for its existence. Therefore, electromagnetic energy can be radiated from the space in which the charged particles are moving, to form

a traveling *electromagnetic wave*. The field equations for the electromagnetic wave can be derived directly from Maxwell's equations.

Consider the light waves radiated by a point source of light. When the source is at a large distance from the point of observation, the *spherical waves* radiated by the source may be assumed to be *plane waves*, like the one shown in Figure 6. The electric and magnetic field vectors of the plane wave may be expressed as follows:

$$\mathbf{E} = E_o \mathbf{e} e^{-i\mathbf{k}.\mathbf{r}} e^{i\omega t}$$

$$\mathbf{H} = H_o \mathbf{h} e^{-i\mathbf{k}.\mathbf{r}} e^{i\omega t} \tag{10}$$

where **k** is the wave propagation vector, **r** is the displacement vector that determines the observation point in space, the unit vectors **e** and **h** correspond to the directions of the electric and magnetic fields, respectively, and the complex coefficients E_o and H_o represent the strengths of the electric and magnetic fields, respectively. It is important to note that, in general, the above expressions give **E** and **H** complex values. However, the actual field is determined only by the real components of the field vectors, i.e. Re[**E**] and Re[**H**], and the complex notation is used only for ease of mathematical manipulation. Bearing this point in mind, we will continue to use the complex forms of **E** and **H**.

The first exponential term in the above field equations suggests that the magnitudes of electric and magnetic fields vary sinusoidally as a function of the distance along the direction of propagation. The direction of the vector **k** corresponds to the direction of propagation of the wave, while its magnitude k, called the *propagation constant*, determines the spatial frequency of the wave. The propagation constant is related to the wavelength λ of the plane wave as follows:

$$k = \frac{2\pi}{\lambda}. \tag{11}$$

If the wavelength lies between 400 nano-meters and 700 nano-meters, the wave can be detected by the human eye and is called *monochromatic light*.

The second exponential term in the field equations indicates that the field intensities also vary sinusoidally as a function of time at a radian frequency of oscillation, ω. The functions that describe the spatial and temporal field variations are dependent on the function that represents the forces applied to the charged particles to generate the wave. In most engineering applications dealing with plane waves, the field is considered to be sinusoidal steady state. Using Maxwell's equations, it can be shown that the unit vectors **e** and **h** are orthogonal to each other and both these vectors are orthogonal to the propagation vector **k**. The direction of either **e** or **h** determines the *polarization* of the plane wave. In Figure 6, the plane wave is shown at a particular instant in time. At that instant, all points on the plane P experience the same electric and magnetic field intensities, namely, E' and H', respectively. Therefore, the plane wave can be thought of as being constituted of infinitely large "equi-field" planes, where each plane is perpendicular to the propagation direction **k**.
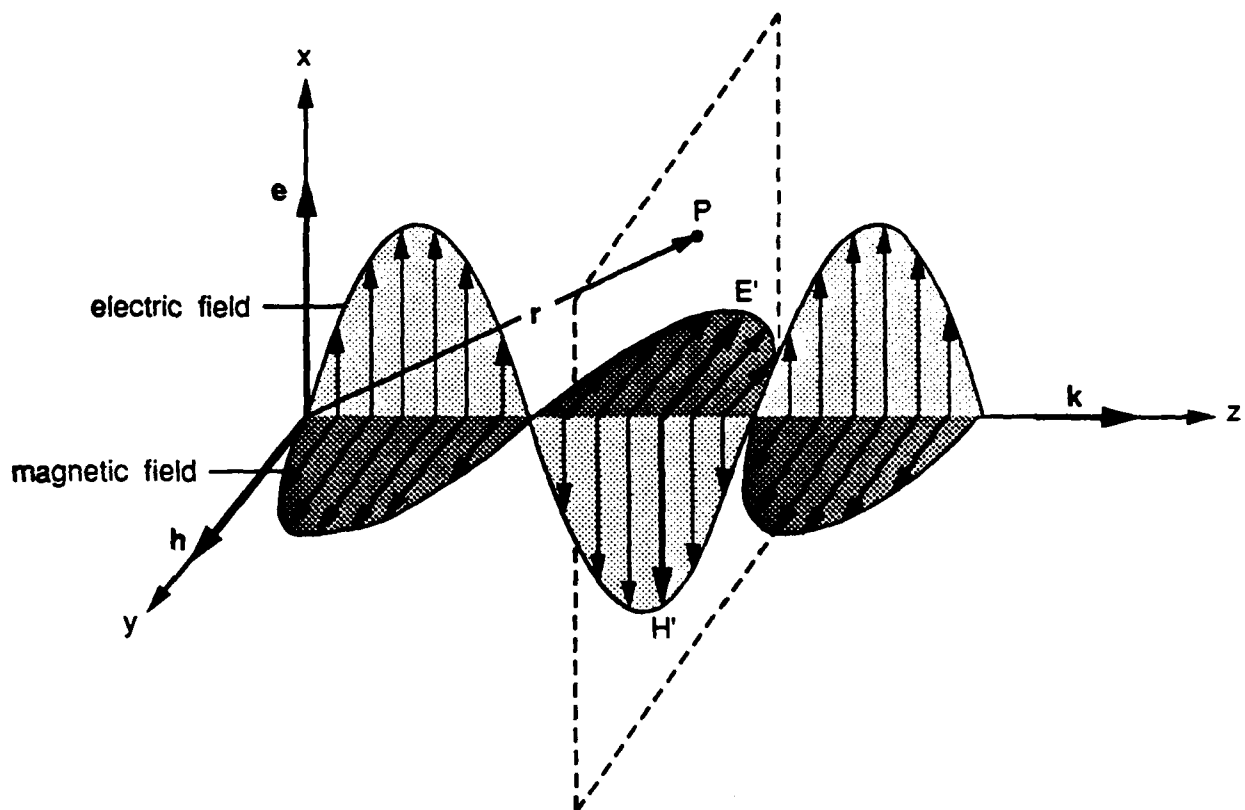
11

Figure 6: A plane electromagnetic wave.

Since time variations in the electric field are the cause of the magnetic field, and vice-versa, the amplitudes E_o and H_o of the two fields are dependent on each other, and are related as follows:

$$H_o = \sqrt{\frac{\epsilon}{\mu}} E_o \, , \tag{12}$$

where ϵ and μ are the *permittivity* and *permeability* of the medium, respectively. The coefficient $\sqrt{\epsilon/\mu}$ is often referred to as the *wave impedance* of the medium. Due to the above stated dependencies between the electric and magnetic field vectors, we see that an electromagnetic wave is completely defined by *either* of the two field vectors, **E** or **H**.

While studying surface reflection, we will be interested in determining the energy of light reflected by the surface in various directions. However, as we will see shortly, reflection models based on physical optics estimate the electromagnetic field scattered by the surface rather than the energy. Therefore, a relationship between the field and the energy carried by an electromagnetic wave would be useful. The rate of flow of *complex energy* per unit

12

area in an electromagnetic wave can be described by a vector S called the *complex Poynting vector* [2]. S is defined as:

$$S = E \times H^*,$$ (13)

and the quantity

$$S_a = \text{Re}[S] = \frac{1}{2}\text{Re}[E \times H^*]$$ (14)

defines the time-averaged rate of flow of *physical energy* per unit area and has the dimensions watts/meter^2. Let E, H, and S_a be the scalar values of the E, H, and S_a, respectively. Then the average rate of flow of energy per unit area is determined from equations 14 and 12 as:

$$S_a = \frac{1}{2}\sqrt{\frac{\mu}{\varepsilon}}EE^* = \frac{1}{2}\sqrt{\frac{\varepsilon}{\mu}}HH^*.$$ (15)

This equation will be used later to find the radiance of a surface from the electromagnetic field scattered by the surface.

4.1.2 Beckmann-Spizzichino Model

The Beckmann-Spizzichino model uses physical optics to describe the reflection of plane waves from smooth and rough surfaces. Owing to the electromagnetic character of light, this model is directly applicable to the reflection of light by surfaces. A detailed derivation of this model can be found in [1]. Our intention is to highlight the key steps involved in the derivation of the model and to clearly state the assumptions made during its development. Later, we will study the reflectance curves predicted by the model for surfaces of differing roughness.

Consider a plane wave incident on a surface, as shown in Figure 7. All vectors and surface points are defined using the Cartesian coordinates x, y, z with origin O and unit vectors x, y, and z. The height of the surface is determined by the function $h = h(x,y)$, and the mean level of the surface is the plane $z = 0$. The location of a surface point Q is described by its displacement vector r:

$$r = xx + yy + h(x,y)z.$$ (16)

All quantities associated with the incident field will be denoted by the subscript 1 and all those associated with the scattered field by the subscript 2. We will represent the plane wave by its electric field intensity only, keeping in mind that the magnetic field intensity may be determined from the electric field. The incident field at the surface point Q may be written as:

$$E_1 = E_{o1}\, e_1\, e^{-i k_1 \cdot r}\, e^{i\omega t}$$ (17)

where E_{o1} represents the electric field amplitude, e_1 is the direction of the electric field, k_1 is the wave propagation vector, and ω is the radian frequency of field oscillation.
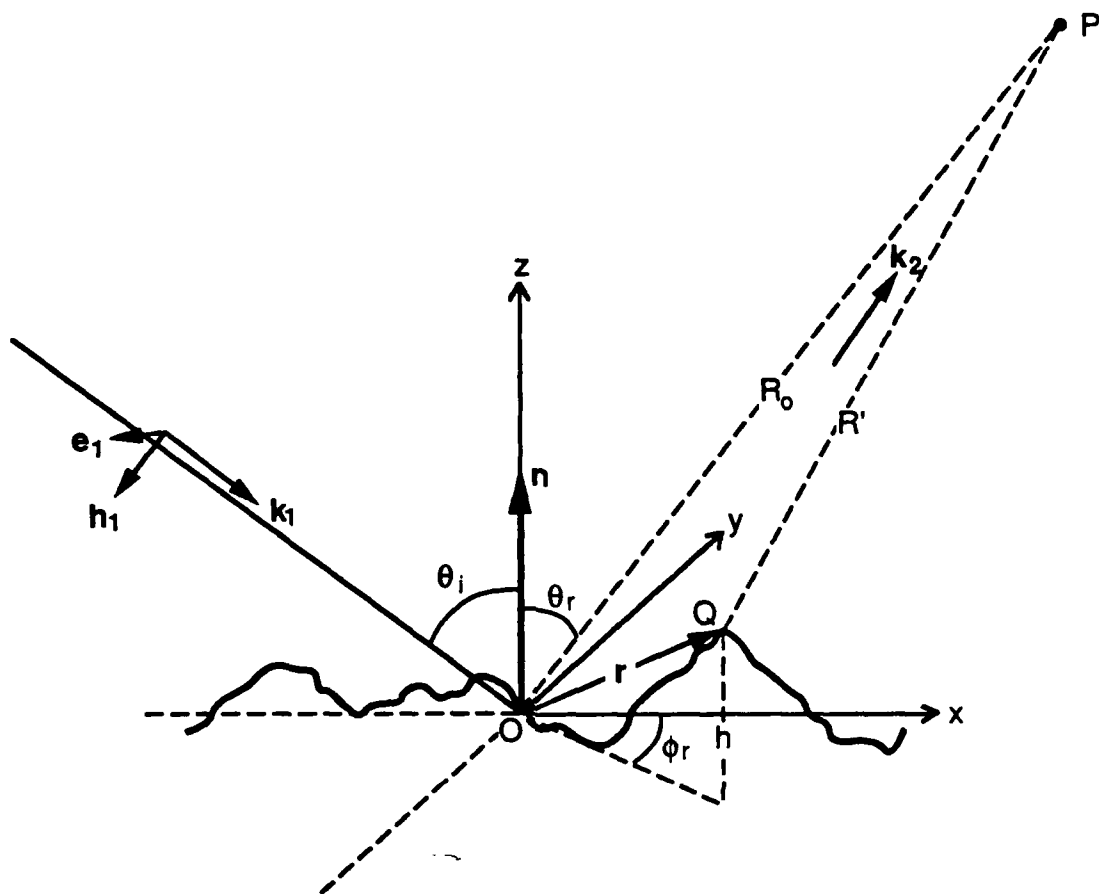
13

Figure 7: A plane wave incident on a rough surface, scattered in various directions.

We are interested in the instantaneous scattering of the incident plane wave by the surface. Hence, we can drop the second exponential term in the above equation, which represents the temporal variation of the incident field. The incident propagation vector k_1 will be assumed to always lie in the x-z plane of the coordinate frame. The angle of incidence θ_i of the plane wave is the angle between the propagation vector k_1 and the z axis of our coordinate frame. If we are interested in the field scattered by the surface in the direction k_2, the corresponding scattering angle θ_r is the angle between k_2 and the z axis. For scattering directions that lie outside the *plane of incidence* (k_1, z), we must introduce an additional angle ϕ_r, as shown in Figure 7. The propagation constant k corresponding to the propagation vectors k_1 and k_2 is related to the wavelength λ of the incident wave by equation 11.

The polarization of the incident wave is determined by the direction of the vector e_1. For parallel polarization, e_1 lies in the the plane of incidence; for perpendicular polarization, e_1 is normal to the plane of incidence. An unpolarized incident wave is one whose e_1 vector

14

is neither parallel nor perpendicular to the plane of incidence, and in general, can vary in direction as a function of time. We will see later how the polarization of the incident field E_1 affects the intensity of the scattered field E_2. We will not, however, concern ourselves with the polarization of the scattered field E_2, as we are only interested in the intensity of E_2. From here on, we will assume the polarization of the incident wave to be either parallel or perpendicular, and the incident field will be denoted by the scalar E_I, where:

$$E_I = \mathbf{e}_1.\mathbf{E}_1 . \tag{18}$$

What happens when the incident plane wave strikes the surface? A simplistic description of the physical situation is as follows. A conducting surface will have an abundance of electrons that are very loosely bound to their atoms. When these electrons are subjected to the electromagnetic field carried by the incident wave, they experience forces. These forces result in a movement of the electrons, often referred to as surface currents. The surface currents give rise to new electromagnetic fields that interact with the incident field to determine the resultant field at the surface. Mathematically, the resultant field $(E)_S$ at a surface point Q must satisfy the *wave equation*[2]:

$$\Delta^2(E)_S + k^2(E)_S = 0, \tag{19}$$

where k is once again the propagation constant. Therefore, the field $(E)_S$ at the surface may be determined by solving the wave equation for the boundary conditions imposed by the surface profile.

The field scattered by the surface in any direction can be determined from the field at the surface. Let P be the point of observation, and let the variable R' denote the distance between P and points on the surface S, as shown in Figure 7. We would like to find the scattered field E_2 at the point P. To this end, let us consider a volume V that is bounded almost everywhere by the surface S but is extended such that the point P lies just outside the volume. Then, it is reasonable to assume that the field $(E)_S$ is continuous, and the above wave equation must therefore be satisfied everywhere inside V. Furthermore, the point inside the volume that is nearest to P will experience almost the same field as the point P. Using these assumptions and Green's first and second theorems, the scattered field E_2 at the point P can be determined [1] from equation 19 as:

$$E_2(P) = \frac{1}{4\pi} \int \int \left((E)_S \frac{\partial \psi}{\partial n} - \psi \left(\frac{\partial E}{\partial n} \right)_S \right) dS, \tag{20}$$

where:

$$\psi = \frac{e^{ikR'}}{R'} . \tag{21}$$

---

[2]It can be shown [2] that for a source-free region of space, Maxwell's equations reduce to the wave equation.

This is called the *Helmholtz integral*, which gives us the solution of the wave equation at any point inside (P is almost inside) a region in terms of the values of the function (surface field $(E)_S$) and its normal derivative on the boundary (the surface S) of the region. A detailed derivation of the Helmholtz integral is provided in [1]. Though it is derived for a closed surface, it is also applicable to open surfaces like the one in Figure 7.

In order to evaluate the above integral, we must find $(E)_S$ and $(\partial E / \partial n)_S$, i.e. the field and its normal derivative on the surface S. In general, these two quantities are unknown. *Kirchoff's assumption* may be used to approximate the values of the field and its normal derivative at each point on the surface. The approximation is obtained by assuming that the surface does not have any sharp edges, and thus the field at a point on the surface is equal to the field that would be present on a tangent plane at that point. Under this assumption, the field on S may be determined as:

$$(E)_S = (1 + F)E_I . \tag{22}$$

And, by differentiating this equation, the normal derivative of the field is determined as:

$$\left(\frac{\partial E}{\partial n}\right)_S = (1 - F)E_I \, \mathbf{k}_1 . \mathbf{n}' , \tag{23}$$

where $\mathbf{n}'$ is the normal to the surface at the point under consideration and F is the *Fresnel reflection coefficient* for a smooth plane.

Consider a plane wave incident on a smooth surface, as shown in Figure 8. As described above, the intensity of the reflected wave is determined by the surface field $(E)_S$, which in turn is dependent on the surface currents. The surface currents induced by the incident wave are determined by the angle of incidence, the polarization of the incident wave, and the electrical properties (permittivity, permeability, and conductivity) of the surface medium. A fraction of the incident electromagnetic energy, determined by these factors, will be reflected by the smooth surface, and the remaining energy transmitted by the surface. The Fresnel reflection coefficient F determines the fraction of incident energy that is reflected by the smooth surface. It is often written as $F(\theta_i', \eta')$, where θ_i' represents the angle of incidence, and η' is the *complex index of refraction* whose value is determined by the electrical properties of the surface medium. In equations 22 and 23, F represents the fraction of the incident field that is reflected by a smooth surface. As we have shown before, the reflected energy may be determined from the reflected field by using equation 15. In deriving their reflectance model, Beckmann and Spizzichino have assumed that the incident wave is of either perpendicular or parallel polarization. The Fresnel coefficients for parallel and perpendicular polarization are, respectively [1]:

$$F_{para} = \frac{Y^2 \cos\theta_i' - \sqrt{(Y^2 - \sin^2\theta_i')}}{Y^2 \cos\theta_i' + \sqrt{(Y^2 - \sin^2\theta_i')}} , \tag{24}$$

incident wave　　　　　　reflected wave

n

θ$_i$　θ$_r$

smooth surface
boundary

θ$_t$

transmitted wave
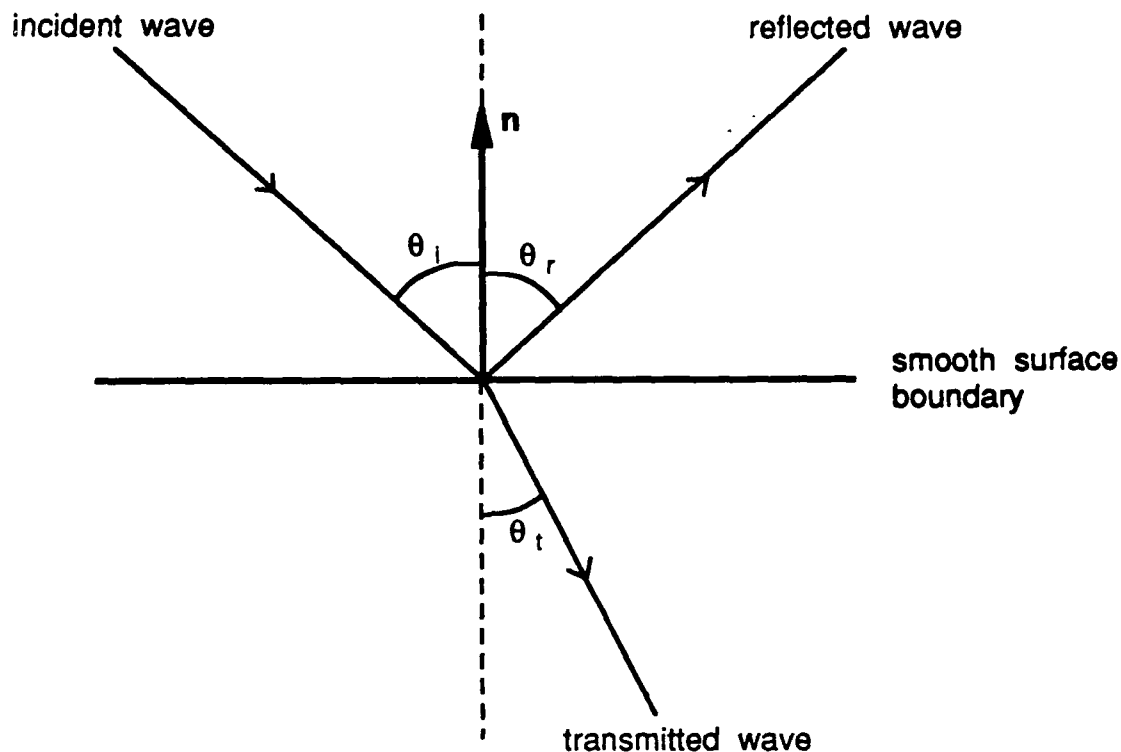
Figure 8: Light waves incident on a smooth surface.

$$F_{perp} = \frac{cos\theta'_i - \sqrt{(Y^2 - sin^2\theta'_i)}}{cos\theta'_i + \sqrt{(Y^2 - sin^2\theta'_i)}} \, . \tag{25}$$

It is important to note the difference between the angle of incidence θ_i shown in Figure 7 and the angle of incidence θ'_i in the above equations. As shown in Figure 9, the angle θ'_i is the "local" angle of incidence, i.e. the angle between the incident wave propagation vector k_1 and the normal vector n' at the surface point under consideration. Therefore, the angle θ'_i will have different values at different points on the surface, while θ_i is constant for a given incident wave. The term Y in the above equations is called the *normalized admittance* of the surface medium and is a function of the complex index of refraction η'. Hence, Y is also a function of the electrical properties of the medium. For a *conductor*, Y approaches infinity, while for a *dielectric* (non-conductor), Y is almost zero.

Let us now return to the problem of finding the scattered field E_2 by evaluating the Helmholtz integral given by equation 20. Let us assume that the surface under consideration is

17
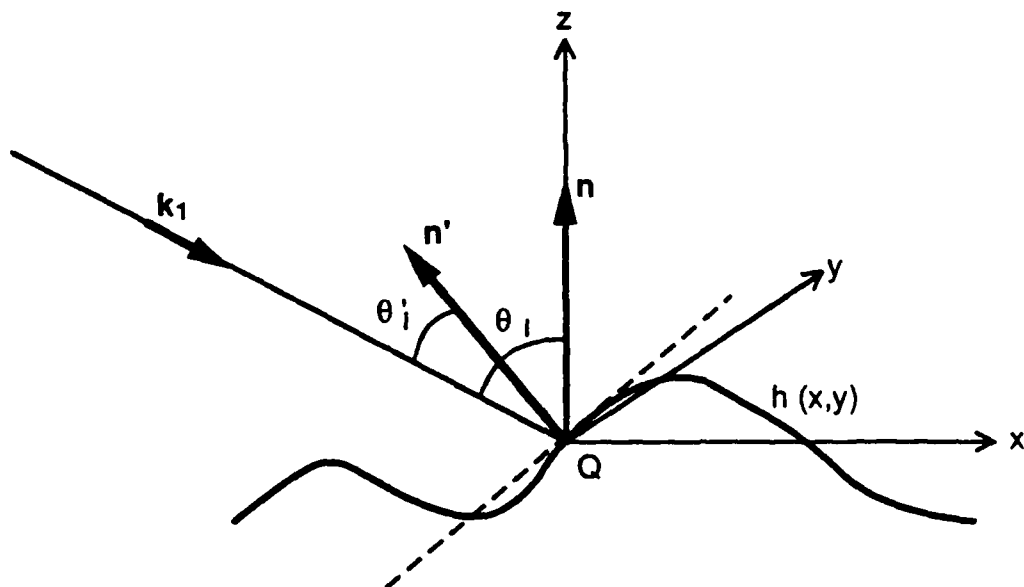
Figure 9: The "local" scattering geometry. The local angle of incidence θ_i' and the local surface orientation n' may differ from the global angle of incidence θ_i and the mean surface orientation n.

a rectangular patch of area A and dimensions $2X$ and $2Y$ in the x and y directions, respectively; i.e. $A = 4XY$. Further, we assume that the observation point P is at a great distance from the surface compared to the physical dimensions of the surface patch and, as a result, the vector k_2 is constant over the entire surface area. Therefore, it can be seen from Figure 7 that, for any surface point, the distance R' can be expressed in terms of the distance R_o and the displacement vector r as:

$$kR' = kR_o - k_2 \cdot r. \tag{26}$$

By substituting equations 22, 23, and 26 in equation 20, we can express the scattered field E_2 as:

$$E_2 = \frac{E_o i k e^{ikR_o}}{4\pi R_o} \int_{-X}^{X} \int_{-Y}^{Y} (a h_x' + c h_y' - b)\, e^{iv \cdot r}\, dx\, dy, \tag{27}$$

where

$$v = (v_x, v_y, v_z) = k(\sin\theta_i - \sin\theta_r \cos\phi_r)x + k(\sin\theta_r \sin\phi_r)y - k(\cos\theta_i + \cos\theta_r)z$$

$$a = (1 - F)\sin\theta_i + (1 + F)\sin\theta_r \cos\phi_r$$

$$b = (1 + F)\cos\theta_r - (1 - F)\cos\theta_i$$

18

$$c = -(1 + F)sin\theta_r sin\phi_r \qquad (28)$$

If the admittance of the surface is finite, we can see from equations 24 and 25 that the Fresnel reflection coefficient F is an involved function of the local angle of incidence θ'_i. For a rough surface, the local orientation will depend on the local slope of the surface. In other words, the factors a, b, and c in equation 27 will not be constant over the surface area. Therefore, for finite admittance, the integral becomes very cumbersome to evaluate, and no solution to the scattering problem is known that is general and exact at the same time. This leads us to our next assumption: the surface medium is considered to be a perfect conductor, i.e. $Y \rightarrow \infty$. From equations 24 and 25, we then see that:

$$F_{para} = 1, \text{ and } F_{perp} = -1 \qquad (29)$$

and the terms a, b, and c in equation 27 are independent of x and y. We also assume the incident wave to be of perpendicular polarization, i.e. $F = F_{perp} = -1$.

The terms h'_x and h'_y in equation 27 denote the slopes of the surface $h(x,y)$ in the x and y directions, respectively. If the surface is perfectly smooth, we see that $h = 0$, $h'_x = 0$, and $h'_y = 0$. A perfectly smooth surface will reflect light only in the *specular* direction $\theta_r = \theta_i$, and for this direction we see that v.r = 0. Therefore, the field E_{2ss} scattered in the specular direction by a smooth perfectly conducting surface is:

$$E_{2ss} = \frac{E_o ike^{ikR_o}}{4\pi R_o} \int_{-X}^{X} \int_{-Y}^{Y} 2\cos\theta_i \, dx \, dy \qquad (30)$$

or:

$$E_{2ss} = \frac{E_o ike^{ikR_o}\cos\theta_i A}{2\pi R_o}. \qquad (31)$$

The magnitude of the field scattered in the specular direction by the smooth perfectly conducting surface is:

$$|E_{2ss}| = \frac{E_o A \cos\theta_i}{\lambda R_o}. \qquad (32)$$

We see that for a perfectly smooth surface, the scattered field is obtained with ease. However, a perfectly smooth surface is only the limiting case of a rough one. We will assume that our surface has random irregularities. By using a statistical model for the irregularities, we can predict the reflection characteristics of the surface. The uncertainty in height of a surface point can be described by a probability distribution function. Though Beckmann and Spizzichino have discussed a variety of distributions, they consider the normal distribution to be the most important and typical of a rough surface.

The normal height distribution model was described in the previous section. The surface height has the mean value $<h> = 0$, standard deviation σ_h, and correlation distance T.

19

The normal distribution $p_h(h)$ is given by equation 4 and the autocorrelation function $C(\tau)$ by equation 5. Since h and the scattered field E_2 are related by equation 27, the statistics of E_2 can be determined from the statistics of h. Beckmann and Spizzichino have derived in detail the mean field and mean power scattered by the surface in an arbitrary direction for any given angle of incidence. They normalize the field and introduce the *scattering coefficient* ρ = E_2/E_{2ss}, and present a detailed derivation of the first and second order statistics of ρ. This normalization gets rid of the factor in front of the integral in equation 27 and helps reduce the number of terms involved in the derivation. Since E_{2ss} is constant, ρ and E_2 are proportional to each other, and the statistics of E_2 can be determined from those of ρ. It turns out that the mean field $<E_2>$ will be non-zero in the specular direction ($\theta_r = \theta_i$) but will tend rapidly toward zero as θ_r deviates from the specular direction. Since $<E_2>$ is a complex quantity, a physical interpretation of its dependency on θ_i and θ_r is not obvious. For example, it does not follow from $<E_2> = 0$ that $<| E_2 |> = 0$. Therefore, Beckmann and Spizzichino have only used $<E_2>$ as a stepping stone to derive the mean scattered power $<E_2E_2^*> = <| E_2 |^2>$. For an incidence angle θ_i, the mean power scattered in the direction (θ_r, ϕ_r) by a rough surface, whose height h is normally distributed with mean value $<h> = 0$, standard deviation σ_h, and correlation distance T, is given by:

$$< E_2E_2^* > = \frac{E_o^2 A^2 \cos^2\theta_i}{\lambda^2 R_o^2} e^{-g} \left(\rho_o^2 + \frac{\pi T^2 D^2}{A} \sum_{m=1}^{m=\infty} \frac{g^m}{m!m} e^{-v_{xy}^2 T^2/4m} \right) , \qquad (33)$$

where

$$g = \left(2\pi \frac{\sigma_h}{\lambda} (\cos\theta_i + \cos\theta_r) \right)^2 \qquad (34)$$

$$\rho_o = sinc\,(v_x X)\, sinc\,(v_y Y) \qquad (35)$$

$$D = \left(\frac{1 + \cos\theta_i \cos\theta_r - \sin\theta_i \sin\theta_r \cos\phi_r}{\cos\theta_i (\cos\theta_i + \cos\theta_r)} \right) \qquad (36)$$

$$v_{xy} = \sqrt{v_x^2 + v_y^2} \qquad (37)$$

In the previous section, the Raleigh criterion was described to illustrate how the roughness of a surface is related to the wavelength of incident light. We see from equation 34 that the factor g in equation 33 is proportional to the square of σ_h/λ. Therefore, g represents the roughness of the surface, and the three cases $g \ll 1$, $g \approx 1$, and $g \gg 1$ correspond to *smooth surfaces*[3], *moderately rough surfaces*, and *rough surfaces*, respectively. It is important to note that the model under consideration only attempts to describe the reflection mechanism that is often referred to by the vision research community as "specular reflection". As seen from equation 33, the mean scattered power is the sum of two terms. The first term, $e^{-g}\rho_o^2$,

---

[3]We define a smooth surface as one that is either perfectly smooth or "slightly" rough.

20

is the *specular spike* component of the specular reflection. It is seen from equation 35 that when the surface dimensions are small, ρ_o becomes a very sharp function of θ_i and θ_r, and is equal to zero for all scattering directions except a very narrow range around the specular direction. Since the mean slope of the surface is constant and is independent of the roughness of the surface, a privileged scattering in the specular direction is expected. The second term in equation 33 corresponds to the *specular lobe*[4], i.e. the diffusely scattered field that results from the roughness of the surface. As we will see shortly, the specular lobe component is distributed around the specular direction. For a perfectly smooth surface, $g = 0$ and the specular lobe vanishes, while the specular spike is strong. As the roughness measure g increases, the spike component shrinks rapidly, while the lobe component increases in magnitude. The exponential series given by the summation in the lobe component may be approximated for smooth ($g \ll 1$) and very rough ($g \gg 1$) surfaces. The approximations result in simpler expressions for the scattered power for these two extreme surface conditions:

$$< E_2 E_2^* >_{smooth} = \frac{E_o^2 A^2 \cos^2\theta_i}{\lambda^2 R_o^2} e^{-g} \left(\rho_o^2 + \frac{\pi T^2 D^2 g}{A} e^{-v_{xy}^2 T^2/4} \right) \qquad (g \ll 1)(38)$$

$$< E_2 E_2^* >_{rough} = \frac{E_o^2 A \cos^2\theta_i \pi T^2 D^2}{\lambda^2 R_o^2 v_z^2 \sigma_h^2} \exp\left(\frac{-v_{xy}^2 T^2}{4 v_z^2 \sigma_h^2} \right) \qquad (g \gg 1) \quad (39)$$

The above equations for scattered power represent the Beckmann-Spizzichino reflectance model. Before we study the reflectance curves predicted by this model, it is important to understand the conditions that ensure the validity of the model. We therefore summarize the assumptions we have made during the derivation of the model and discuss the restrictions imposed by these assumptions.

4.1.3 Assumptions and Related Comments

- The surface height is assumed to be normally distributed. However, Beckmann and Spizzichino have derived reflectance models for surfaces with other height distributions, and also surfaces with periodic profiles.

- The radius of curvature of surface irregularities is large compared to the wavelength of incident light (Kirchoff's assumption). This assumption is required to approximate the electromagnetic field and its normal derivative on the surface. The approximation will break down if the surface irregularities include sharp edges or sharp points.

---

[4]Beckmann and Spizzichino have referred to this component as the "diffuse" component. The term "diffuse" has historically been used by the vision community to describe the reflection component that results from other mechanisms such as multiple reflections and internal scattering. To avoid confusion we will refer to the diffuse component of specular reflection as the specular lobe.

- The surface is assumed to be a perfect conductor. This assumption forces the quantities *a*, *b*, and *c* in equation 27 to be constants, thus making it easier to evaluate the Helmholtz integral. Beckmann and Spizzichino claim that this assumption is not as severe as it may first appear and that surface roughness has a greater effect on the scattered field than the electrical properties of the surface medium. Moreover, it is possible to approximate the scattered field and power for finite conductors by averaging the Fresnel coefficient *F* over the entire surface area and using the resultant value <*F*> as a constant in the Helmholtz integral. This way the mean field and mean power scattered by a finite conductor are found [1] to be

$$< E_2 >_f \; = \; < F > < E_2 >_\infty \tag{40}$$

$$< E_2 E_2^* >_f \; = \; < FF^* > < E_2 E_2^* >_\infty , \tag{41}$$

where the indices *f* and ∞ denote finite and infinite conductivity, respectively.

- We have ignored the *masking* and *shadowing* of surface points by adjacent surface points. Adjacent points may obstruct either the wave incident at a given point or the waves scattered from it. Clearly, these effects are functions of the angles of incidence and reflection. It is possible to compensate for the shadowing and masking effects by replacing the height function $h(x,y)$ by $S(x,y)h(x,y)$, where $S(x,y)$ is the shadowing function [27] that tends toward unity for surface points that are illuminated and zero for those that are not.

- We have assumed that the incident wave is reflected only once and does not bounce between surface points before it is scattered in the direction of the observation point *P*. Without this assumption it would be very difficult to compute the scattered field; no closed-form solution that takes *multiple scatterings* into account is known at the present time.

- The incident wave is assumed to be perpendicularly polarized. The mean field and power can also be determined for parallel polarization. Beckmann and Spizzichino have also discussed possible approaches to solving the scattering problem when the polarization vector e_1 of the incident wave is neither parallel nor perpendicular to the plane of incidence.

- The incident wave is assumed to be a plane wave. This assumption is reasonable when the source is at a great distance from the surface, relative to the physical dimensions of the surface. If the source is relatively close to the surface, the incident waves must be considered to be spherical waves. We have also assumed the observation point to be sufficiently far removed from the surface to regard the scattered waves as plane waves.

22

4.1.4 Surface Radiance and Image Irradiance from Scattered Field

The physical optics reflection model predicts the mean field and mean power scattered by a rough surface. We are interested in the radiance of the surface since we know that radiance can be related to image irradiance [10]. Radiance was defined in Section 2 as:

$$L_r = \frac{d^2 \Phi_r}{d\omega_r \, dA_s \cos\theta_r} . \qquad (42)$$
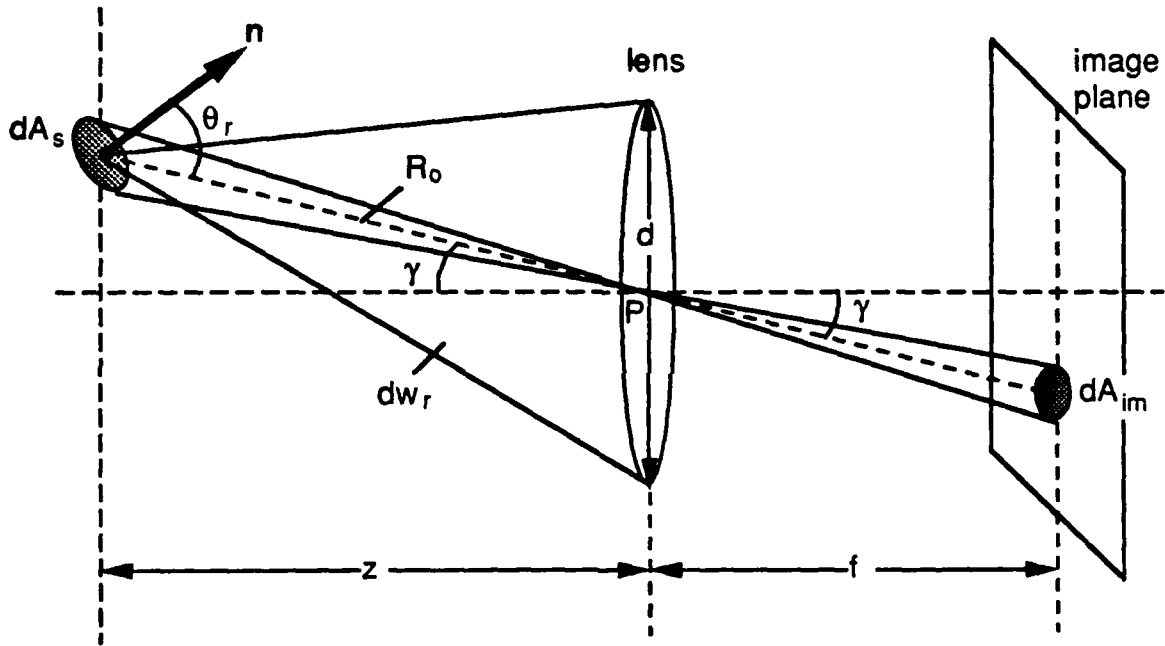
Consider the image formation geometry shown in Figure 10. For convenience, we will use

Figure 10: Image formation: light waves radiated by the surface area dA_s and gathered by the lens are projected onto an area dA_{im} on the image plane. Adapted from [10].

the areas and solid angles shown in the figure to determine the surface radiance. The surface element dA_s is projected by the lens onto an area dA_{im} on the image plane. Since the solid angles subtended from the center P of the lens by both areas dA_s and dA_{im} are equal, we can relate the two areas as:

$$dA_s = \frac{dA_{im} \cos\gamma}{\cos\theta_r} \left(\frac{z}{f}\right)^2 . \qquad (43)$$

As the viewing direction θ_r changes, we see that the surface area dA_s that is projected onto the same image element (pixel) area changes as a function of θ_r. Since the image element

23

area dA_{im} is constant for a given sensor, the surface area dA_s must be determined from dA_{im}. All light rays radiated from dA_s that are incident on the lens area dA_l are projected onto the image area dA_{im}. Therefore, $d\omega_r$ in equation 42 corresponds to the solid angle subtended by the lens when viewed from from the area dA_s, and is determined as:

$$d\omega_r = \frac{dA_l \cos\gamma}{R_o^2}. \tag{44}$$

The flux $d^2\Phi_r$ in equation 42 is the energy of light received by the lens area dA_l, and can be determined from equation 15 as:

$$d^2\Phi_r = S_a \, dA_l \cos\gamma = \frac{1}{2}\sqrt{\frac{\mu}{\varepsilon}} < E_2 E_2^* > dA_l \cos\gamma. \tag{45}$$

By substituting equations 43, 44, and 45 into equation 42, we obtain:

$$L_r = \frac{1}{2}\sqrt{\frac{\mu}{\varepsilon}}\frac{R_o^2 f^2 < E_2 E_2^* >}{z^2 \, dA_{im} \cos\gamma}. \tag{46}$$

It is not possible to determine the exact value of the radiance from the statistics of the scattered field. The radiance L_r in the above equation is actually the mean (expected) radiance, $<L_r>$. The mean scattered power $<E_2 E_2^*>$ was determined as an integral over the entire area of the surface. In Figure 10, we see that the image element dA_{im} receives light radiated only by the surface element dA_s and, therefore, the mean scattered power must be computed as an integral over the surface area $A = dA_s$. Since the image element area dA_{im} is constant for all viewing directions θ_r, the area of integration dA_s is determined by equation 43. Thus, for a given incidence angle θ_i, the radiance in the direction (θ_r, ϕ_r) of a rough surface, whose height h is normally distributed with mean value $<h> = 0$, standard deviation σ_h, and correlation distance T, is given as:

$$L_r = \sqrt{\frac{\mu}{\varepsilon}}\frac{E_o^2 \cos^2\theta_i}{2\lambda^2} e^{-g} \left(\left(\frac{z}{f}\right)^2 \frac{dA_{im} \cos\gamma}{\cos^2\theta_r}\rho_o^2 + \frac{\pi T^2 D^2}{\cos\theta_r}\sum_{m=1}^{m=\infty}\frac{g^m}{m!m} e^{-v_{xy}^2 T^2/4m} \right) \tag{47}$$

Similarly, from equations (38) and (39), the surface radiance for smooth and rough surfaces may be written as

$$L_{rsmooth} = \sqrt{\frac{\mu}{\varepsilon}}\frac{E_o^2 \cos^2\theta_i}{2\lambda^2} e^{-g} \left(\left(\frac{z}{f}\right)^2 \frac{dA_{im} \cos\gamma}{\cos^2\theta_r}\rho_o^2 + \frac{\pi T^2 D^2 g}{\cos\theta_r} \right) \quad (g \ll 1)(48)$$

$$L_{rrough} = \sqrt{\frac{\mu}{\varepsilon}}\frac{E_o^2 \cos^2\theta_i \, \pi T^2 D^2}{2\lambda^2 \cos\theta_r v_z^2 \sigma_h^2} exp\left(\frac{-v_{xy}^2 T^2}{4v_z^2\sigma_h^2}\right) \quad (g \gg 1) \tag{49}$$

As stated in Section 2, we can also obtain the BRDF, $f_r(\theta_i; \theta_r, \phi_r)$ of the surface from its radiance and irradiance. From Section 2, we see that surface irradiance I_s is defined as

24

the light energy incident per unit area of the surface. If E_I is the scalar value of the incident plane wave $\mathbf{E_1}$, the surface irradiance can be obtained by once again using equation 15:

$$I_s = S_a \cos\theta_i = \frac{1}{2}\sqrt{\frac{\mu}{\varepsilon}} < E_I E_I^* > \cos\theta_i \qquad (50)$$

where the term $\cos\theta_i$ accounts for the fact that the same amount of incident energy is received by a greater surface area when the angle of incidence θ_i is increased. Hence, the BRDF of the surface is determined using equations 47 and 50 as $f_r = L_r/I_s$.

Using the imaging geometry shown in Figure 10, Horn [10] has established a relationship between surface radiance L_r and image irradiance I_{im}. The image irradiance is found to be proportional to surface radiance and is given by:

$$I_{im} = L_r \frac{\pi}{4} \left(\frac{d}{f}\right)^2 \cos^4\gamma . \qquad (51)$$

When the image covers only a narrow angle of the scene, we see that $\gamma \approx 0$ and it is reasonable to assume that $\cos\gamma = 1$ in the above equations.

4.1.5 Radiance Diagrams

The performance of a physical optics reflectance model is usually illustrated by *scattering diagrams* [1] in which either the scattered field or the scattered power is plotted as a function of the source and viewing angles. In radiometry, surface reflectance is often represented by the BRDF $f_r(\theta_i; \theta_r, \phi_r)$ normalized by the BRDF, f_{r_o}, in the specular direction [30]. Since we are interested in interpreting image irradiance values, however, and since image irradiance is proportional to surface radiance, we will illustrate surface reflectance properties by *radiance diagrams*, where *absolute* surface radiance is plotted as a function of viewing angle (θ_r, ϕ_r) and incidence angle θ_i. Radiance diagrams will be plotted for different values of the surface roughness parameters. For simplicity, we will assume that the observation point P lies in the plane of incidence, i.e. $\phi_r = 0$. In this section, we will plot radiance as a function of the viewing angle θ_r for fixed values of the incidence angle θ_i. Later, we will investigate how the radiance changes as a function of θ_i, for fixed values of θ_r.

As mentioned earlier, the parameter g in equation 47 represents the roughness of the surface. We see from equation 34 that g is a function of the ratio σ_h/λ. In Section 3 we have also seen that the shape of a normally distributed surface can be represented by the ratio σ_h/T. We would like to see how the radiance diagram changes with the two ratios σ_h/λ and σ_h/T. We will vary the values of the two ratios by keeping σ_h constant and varying λ and T. Figure 11 shows radiance diagrams for different values of σ_h/λ. All the radiance diagrams are generated by using the general radiance expression given by equation 47. The specular lobe component of the radiance was computed by summing the first 100 terms of the

25

exponential series. In Figure 11a, we see that $\sigma_h/\lambda = 0.002$, i.e. $g \approx 0$. From equation 47 we see that when $g \approx 0$, the lobe component is near zero and the spike component is dominant. The surface behaves in a mirror-like manner and reflects light only in the specular direction $\theta_r = \theta_i$. Also note that the radiance in the specular direction is constant for different values of θ_i. This is consistent with our real-world experience; when we look at a perfect mirror from the specular angle, we see a virtual image of the source. Further, the image appears the same irrespective of the angle of incidence. We have found that this mirror-like behavior is observed when $\sigma_h/\lambda < 0.025$. In Figure 11a, the spike component look like a delta function. However, from equation 35 we see that the spike component is really a *sinc* function. This is seen in Figure 11b, where one of the radiance curves in Figure 11a is magnified.

As σ_h/λ is increased above the value 0.025 (Figures 11c and 11d), we find that the spike component decreases rapidly in magnitude[5]. However, the spike component is still very strong for large values of θ_r and θ_i. This is because g (equation 34) is a function not only of σ_h/λ, but also of $(cos\theta_i + cos\theta_r)$. Therefore, for large values of θ_i and θ_r, g approaches zero, the spike component increases, and the surface tends to behave like a mirror. However, we see that when σ_h/λ is increased further (Figures 11e and 11f), the spike component fades away, and the lobe component begins to dominate the radiance value. We have found that when $\sigma_h/\lambda > 1.5$, the spike component disappears, and the radiance value is determined solely by the lobe component.

Figure 12 and Figure 13 illustrate how the radiance diagram is affected by the surface roughness ratio σ_h/T. For the radiance diagrams in Figure 12, $\sigma_h/\lambda = 0.002$. We see that the spike component is unaffected by changes in the correlation distance T. In other words, for a given wavelength of incident light, the spike component would be the same for two surfaces with different shapes but the same root-mean-square height σ_h. However, in Figure 13 we see that the shape and magnitude of the lobe component are greatly dependent on the ratio σ_h/T.

In Figure 13a, we compare the radiance diagrams generated by using the general radiance expression (equation 47) and the approximate radiance expression for rough surfaces (equation 49) for $\sigma_h/\lambda = 10.0$ and $\sigma_h/T = 0.1$. We see that the expression L_{rrough} approximates the lobe component of the L_r quite well, and may be used when the spike component is negligible. In Figure 13b, we see that the lobe component is sharp and concentrated around the specular direction. We have found that when $\sigma_h/T < 0.02$, the shape of the lobe component resembles that of the spike component. However, the magnitude of the lobe peak increases with the incidence angle θ_i. This effect results from the term $1/cos\theta_r$ in equation 49. From Figure 13c-13f, we see that as the ratio σ_h/T increases, the lobe gets wider and the lobe peak decreases in magnitude. In fact, for $\sigma_h/T < 0.05$ the lobes may be approximated by

---

[5]If the radiance or the BRDF is normalized by the corresponding value in the specular direction, the decrease in the spike component is not observed. It is for this reason that we have chosen to plot the absolute radiance value.
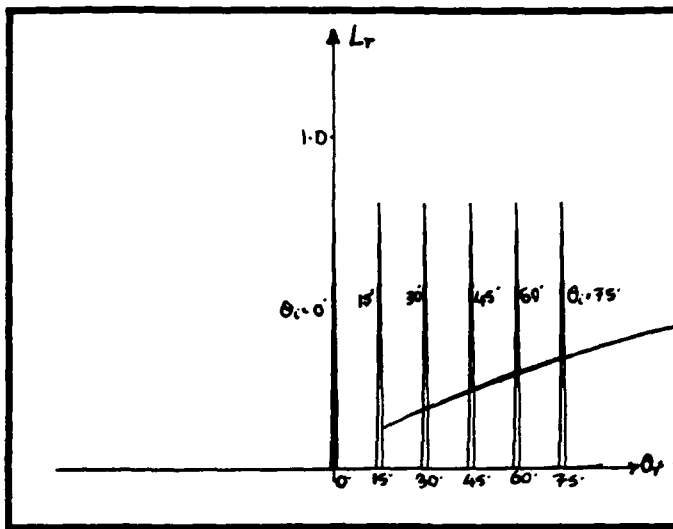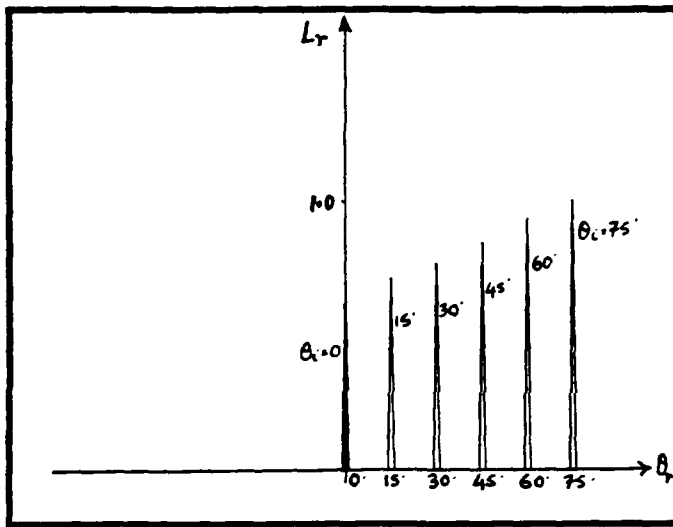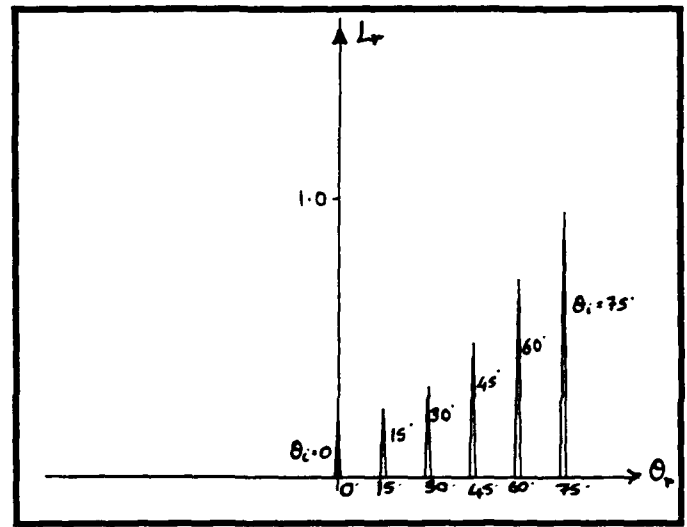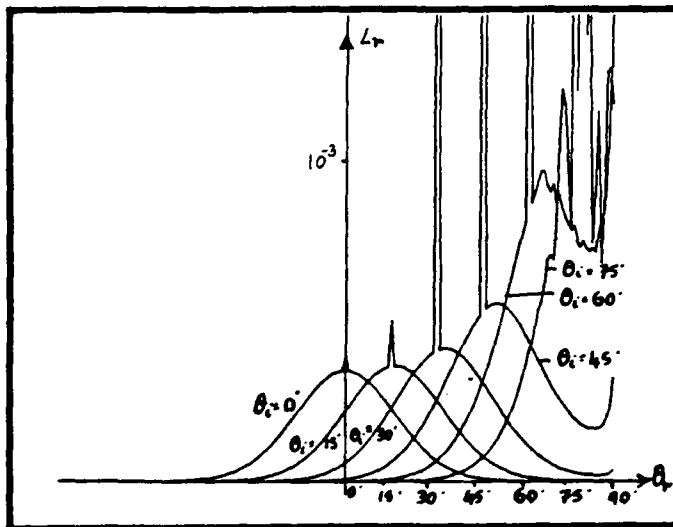
(a) $\sigma_h = 0.001$, $T = 0.01$, $\lambda = 0.5$
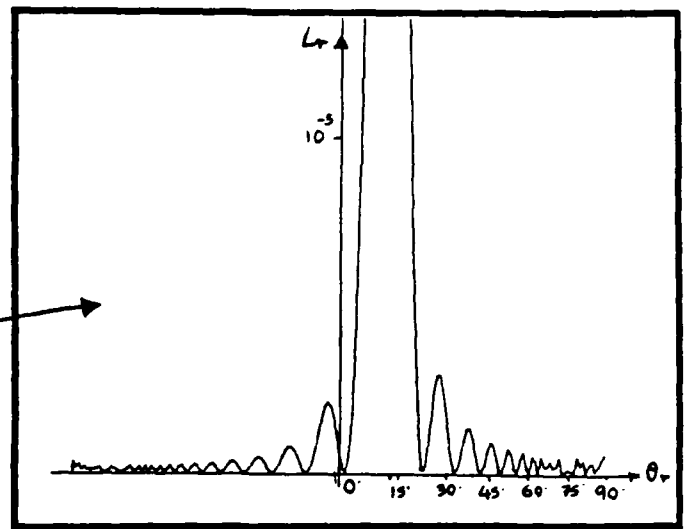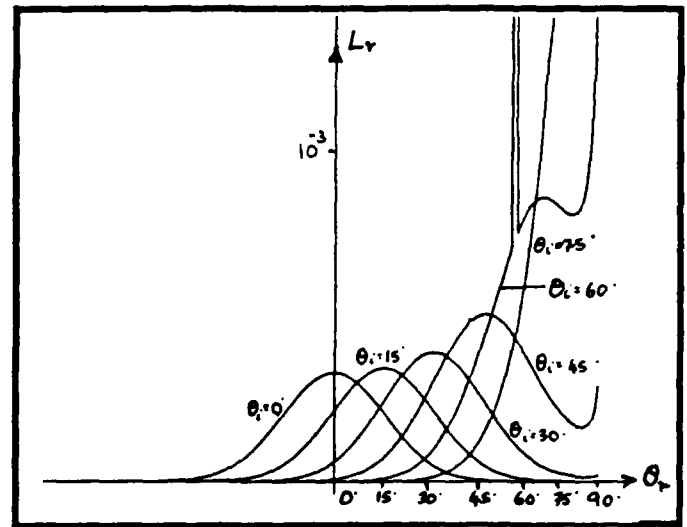
(b)

(c) $\sigma_h = 0.001$, $T = 0.01$, $\lambda = 0.02$

(d) $\sigma_h = 0.001$, $T = 0.01$, $\lambda = 0.01$
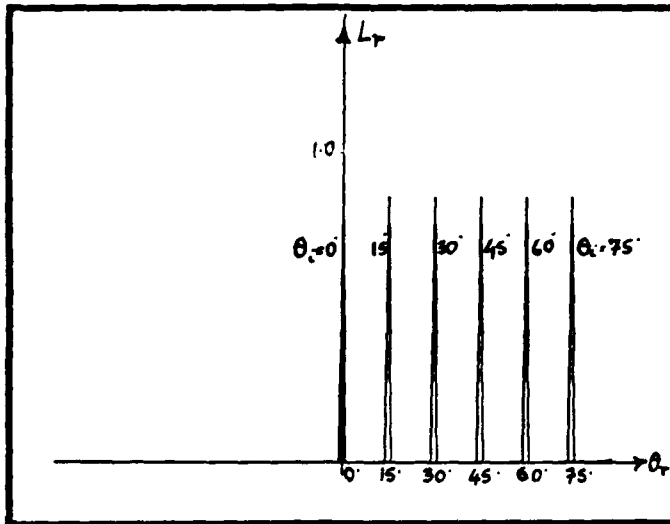
(e) $\sigma_h = 0.001$, $T = 0.01$, $\lambda = 0.003$
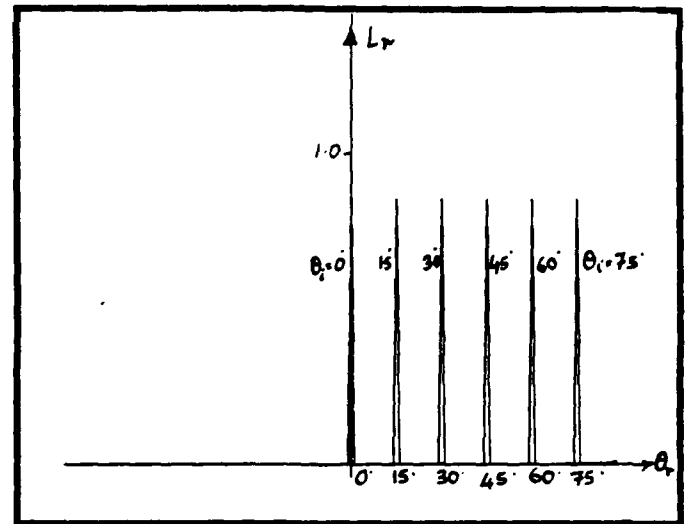
Note change of scale between (d) and (e).
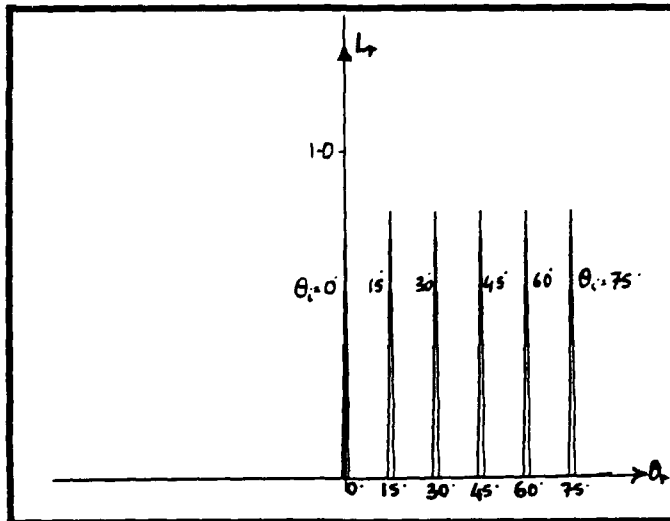
(f) $\sigma_h = 0.001$, $T = 0.01$, $\lambda = 0.002$

Figure 11: Radiance diagrams predicted by the Beckmann-Spizzichino model for different values of σ_h/λ.
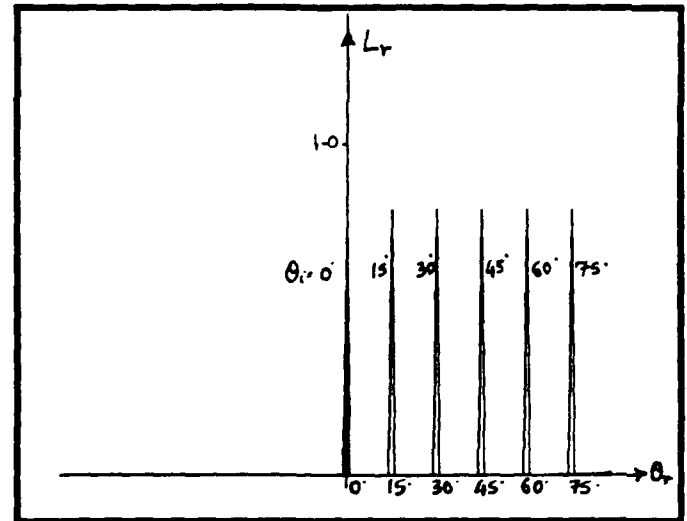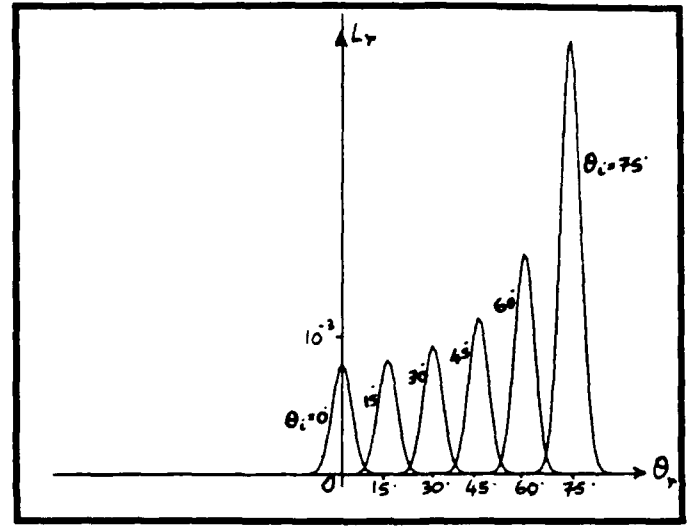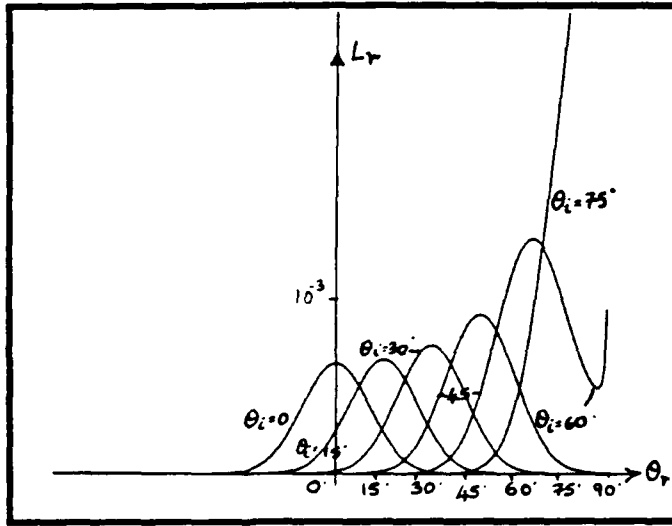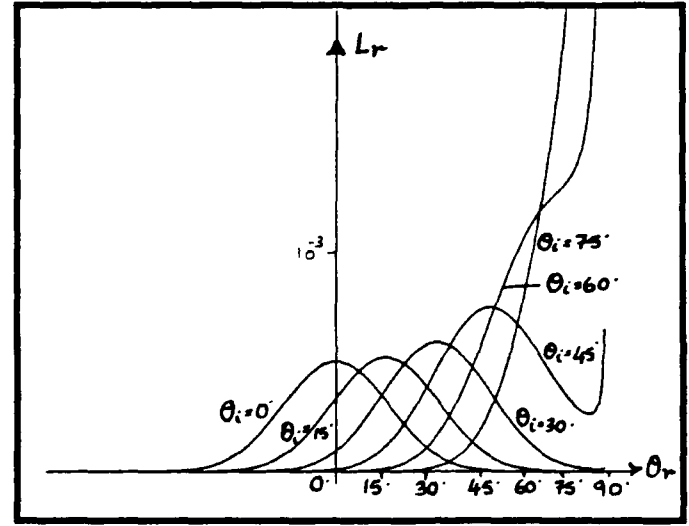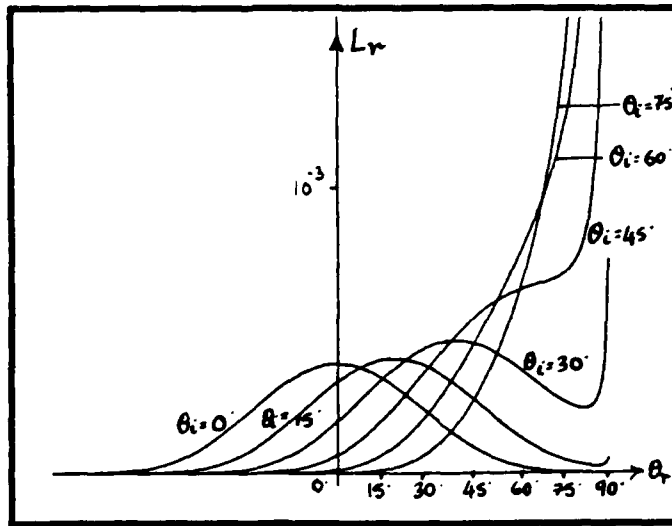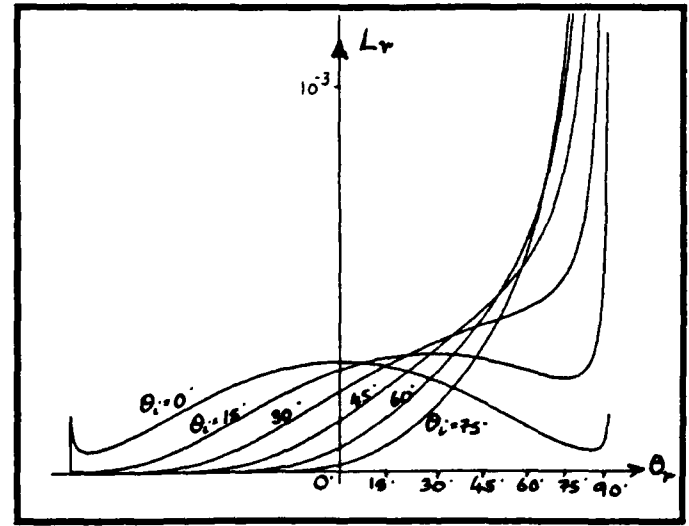
27

(a) $\sigma_h = 0.001$, $T = 0.05$, $\lambda = 0.5$

(b) $\sigma_h = 0.001$, $T = 0.02$, $\lambda = 0.5$

(c) $\sigma_h = 0.001$, $T = 0.01$, $\lambda = 0.5$

(d) $\sigma_h = 0.001$, $T = 0.006$, $\lambda = 0.5$

Figure 12: Radiance diagrams of the specular spike component predicted by the Beckmann-Spizzichino model for different values of σ_h/T.
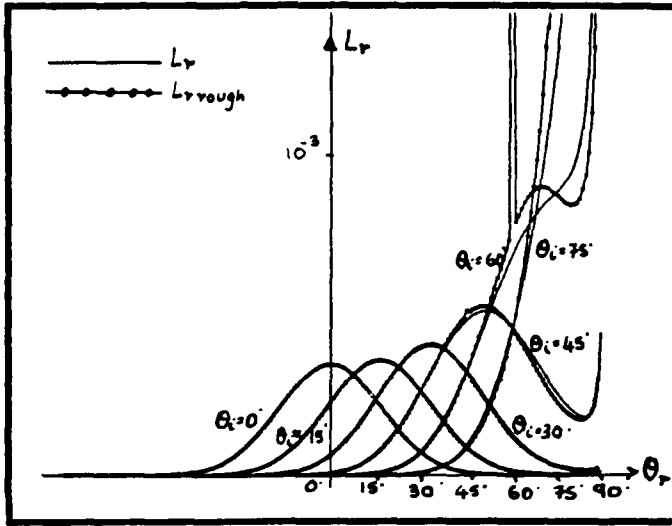
28

Figure 13: Radiance diagrams of the specular lobe component predicted by the Beckmann-Spizzichino model for different values of σ_h/T.

29

Gaussian functions with mean values corresponding to the specular direction $\theta_i = \theta_r$. For larger values of σ_h/T, however, the the lobes tend to peak at viewing angles greater than the specular angle; these are called *off-specular peaks*. Also note that as θ_r approaches 90 degrees, the radiance values approach infinity. By using a shadowing function, this effect can be minimized, while preserving the shape of the radiance curves for smaller values of θ_r.

4.2 Geometrical Optics Model

An outstanding feature of visible light is its short wavelength. Often, the wavelength of incident light is far shorter than the physical dimensions of the surface imperfections it encounters, and in such cases it is possible to solve the problem of reflection in an approximate way. The approximation that is valid for short wavelengths of light is known as *geometrical optics*, and it allows us to treat the reflection problem in a way far simpler than the physical optics approach of solving Maxwell's equations.

In this section, we will discuss the Torrance-Sparrow model, which uses geometrical optics to describe the specular reflection mechanism. To their specular reflection model, Torrance and Sparrow have appended the Lambertian model to account for internal scattering and multiple reflection mechanisms. We will very briefly describe the Lambertian model [6] and proceed to explain the Torrance-Sparrow model, once again highlighting the important steps and assumptions. Later, we will present radiance diagrams predicted by the Torrance-Sparrow model for different surface roughness values, and compare it to the Beckmann-Spizzichino physical optics model.

4.2.1 Lambertian Model

Lambert [15] was the first to investigate the mechanisms underlying diffuse reflection. Surfaces that satisfy Lambert's law appear equally bright from all directions. In other words, the radiance of a Lambertian surface is independent of the viewing direction. Broadly speaking, there are two mechanisms that produce Lambertian reflection. In one case, the light rays that impinge on the surface are reflected many times by surface undulations before they are scattered into space, as shown in Figure 14a. If these *multiple reflections* occur in a random manner, the incident energy is distributed in all directions, resulting in diffuse reflection. Another mechanism leading to Lambertian reflection is the *internal scattering* of light rays. In this case, the light rays penetrate the surface and encounter microscopic inhomogeneities in the surface medium, as shown in Figure 14b. The light rays are repeatedly reflected and refracted at boundaries between regions of differing refractive indices. Some of the scattered

---

[6]Lambertian reflection is normally categorized as "body" reflection rather than surface reflection. The model is discussed here only because it is used later to represent one of the primary reflection components.

rays find their way to the surface with a variety of directions, resulting in diffuse reflection. When diffuse reflection produced by either or both of the above mechanisms produce constant surface radiance in all directions, we have Lambertian reflection.
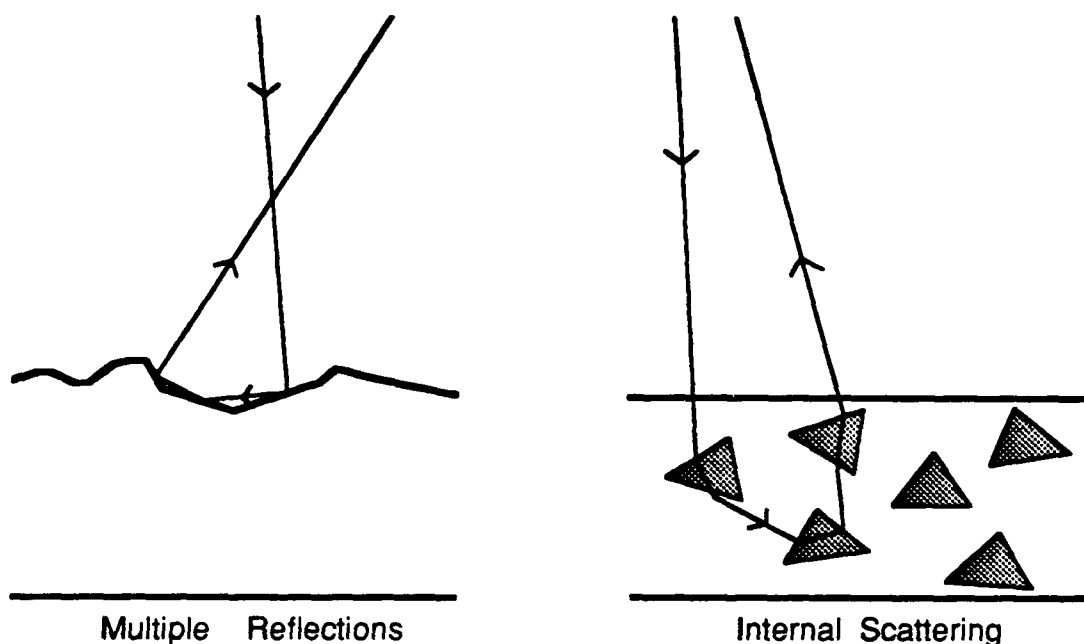

Figure 14: Diffuse reflection resulting from multiple reflection and internal scattering mechanisms.

The surface radiance L_r of a Lambertian surface is proportional to the irradiance I_s (incident energy per unit area) of the surface. Consider an infinitesimal surface area dA_s illuminated by an infinitesimal source area dA_i, as shown in Figure 15. The flux incident on dA_s may be determined from the source radiance L_i as:

$$d^2\Phi_i = L_i \, d\omega_s \, dA_i. \tag{52}$$

From the solid angles subtended by the surface and source areas, we obtain:

$$dA_i = d\omega_i \, r^2, \tag{53}$$

$$d\omega_s = \frac{dA_s \cos\theta_i}{r^2}. \tag{54}$$

31

Substituting equations 53 and 54 into equation 52, we obtain:

$$d^2\Phi_i = L_i \, d\omega_i \, dA_s \, cos\theta_i \, .$$ (55)

The surface irradiance is determined from the above equation as:

$$I_s = \frac{d^2\Phi_i}{dA_s} \, ,$$ (56)

Since surface radiance is proportional to surface irradiance, and since it is meaningful only when it attains positive values, it can be expressed as:

$$L_r = \kappa_{diff} \, max \, [0, \, (L_i \, d\omega_i \, cos\theta_i)] \, ,$$ (57)

where κ_{diff} determines the fraction of the incident energy that is diffusely reflected by the surface.
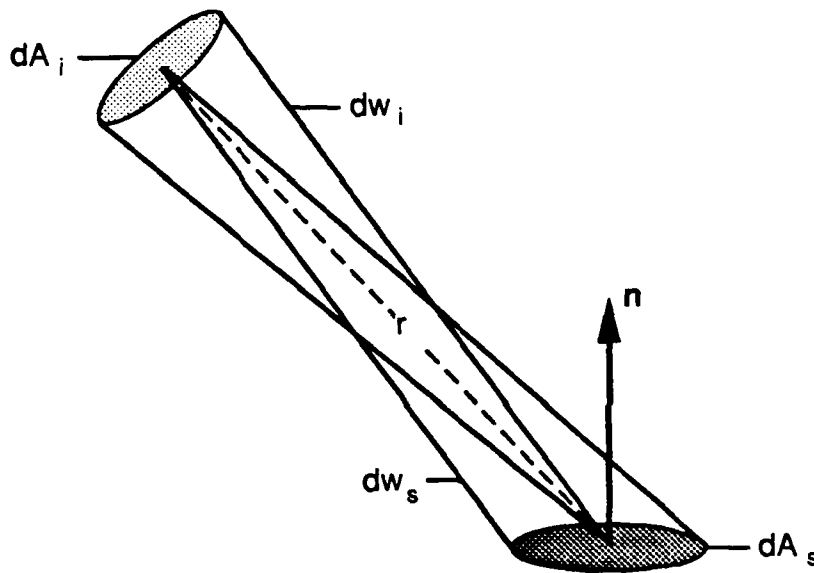
Figure 15: Dependence of the incident light energy on the source direction.

4.2.2 Torrance-Sparrow Model

The Torrance-Sparrow model was developed with the aim of describing the mechanism for specular reflection by rough surfaces. Based on geometrical optics, this model is valid only

32

when the wavelength of light is much smaller than the root-mean-square surface roughness. The surface is modeled as a collection of planar micro-like facets. As explained in Section 3.2, the surface has a mean surface orientation **n**, and the slope α of each planar facet with respect to the mean orientation is described by a probability distribution. Each facet reflects incident light in the specular direction determined by its slope. Since the facet slopes are randomly distributed, light rays are scattered in various directions. Therefore, it is possible to assign a specific distribution function to the facet slopes and determine the radiance of the surface in any given direction.

Torrance and Sparrow have assumed the facet slopes to be normally distributed. Further, they have assumed the distribution to be rotationally symmetric about the mean surface normal **n**. Hence, facet slopes may be represented by a one-dimensional normal distribution:

$$p_\alpha(\alpha) = c\, e^{-\frac{\alpha^2}{2\sigma_\alpha^2}}, \tag{58}$$

where c is a constant, and the facet slope α has mean value $<\alpha> = 0$ and standard deviation σ_α. As we have stated earlier, for this surface model, roughness is represented by the parameter σ_α.

Consider the geometry shown in Figure 16. The surface area dA_s is located at the origin of the coordinate frame, and its surface normal points in the direction of the z-axis. The surface is illuminated by a beam of light that lies in the x-z plane and is incident on the surface at an angle θ_i. We are interested in determining the radiance of the surface in the direction (θ_r, ϕ_r). Only those planar micro-facets whose normal vectors lie within the solid angle $d\omega'$ are capable of specularly reflecting light flux that is incident at the angle θ_i into the infinitesimal solid angle $d\omega_r$. From the angles θ_i, θ_r, and ϕ_r, we can determine the local angle of incidence θ_i' and slope α of the reflecting facets:

$$\theta_i' = \frac{1}{2}\cos^{-1}(\cos\theta_r\cos\theta_i - \sin\theta_r\sin\theta_i\cos\phi_r), \tag{59}$$

$$\alpha = \cos^{-1}(\cos\theta_i\cos\theta_i' + \sin\theta_i\sin\theta_i'\cos(\sin^{-1}(\sin\phi_r\sin\theta_r / \sin 2\theta_i'))). \tag{60}$$

The number of facets per unit area of the surface that are oriented within the solid angle $d\omega'$ is equal to $(p_\alpha(\alpha)\, d\omega')$. Therefore, the number of facets in the surface area dA_s that are oriented within $d\omega'$ is equal to $(p_\alpha(\alpha)\, d\omega'\, dA_s)$. Let a_f be the area of each facet. Then, the area of points in dA_s that will reflect light from the direction θ_i into the solid angle $d\omega_r$ is equal to $(a_f\, p_\alpha(\alpha)\, d\omega'\, dA_s)$. All the reflecting facets are assumed to have the same local angle of incidence, θ_i'. From equation 55, the flux incident on the set of reflecting facets is determined as:

$$d^2\Phi_i = L_i\, d\omega_i\, (a_f p_\alpha(\alpha)\, d\omega'\, dA_s)\cos\theta_i'. \tag{61}$$

The fraction of incident light that is reflected by each planar facet is determined by the Fresnel reflection coefficient. The Fresnel coefficients $F_{para}(\theta_i', \eta')$ and $F_{perp}(\theta_i', \eta')$
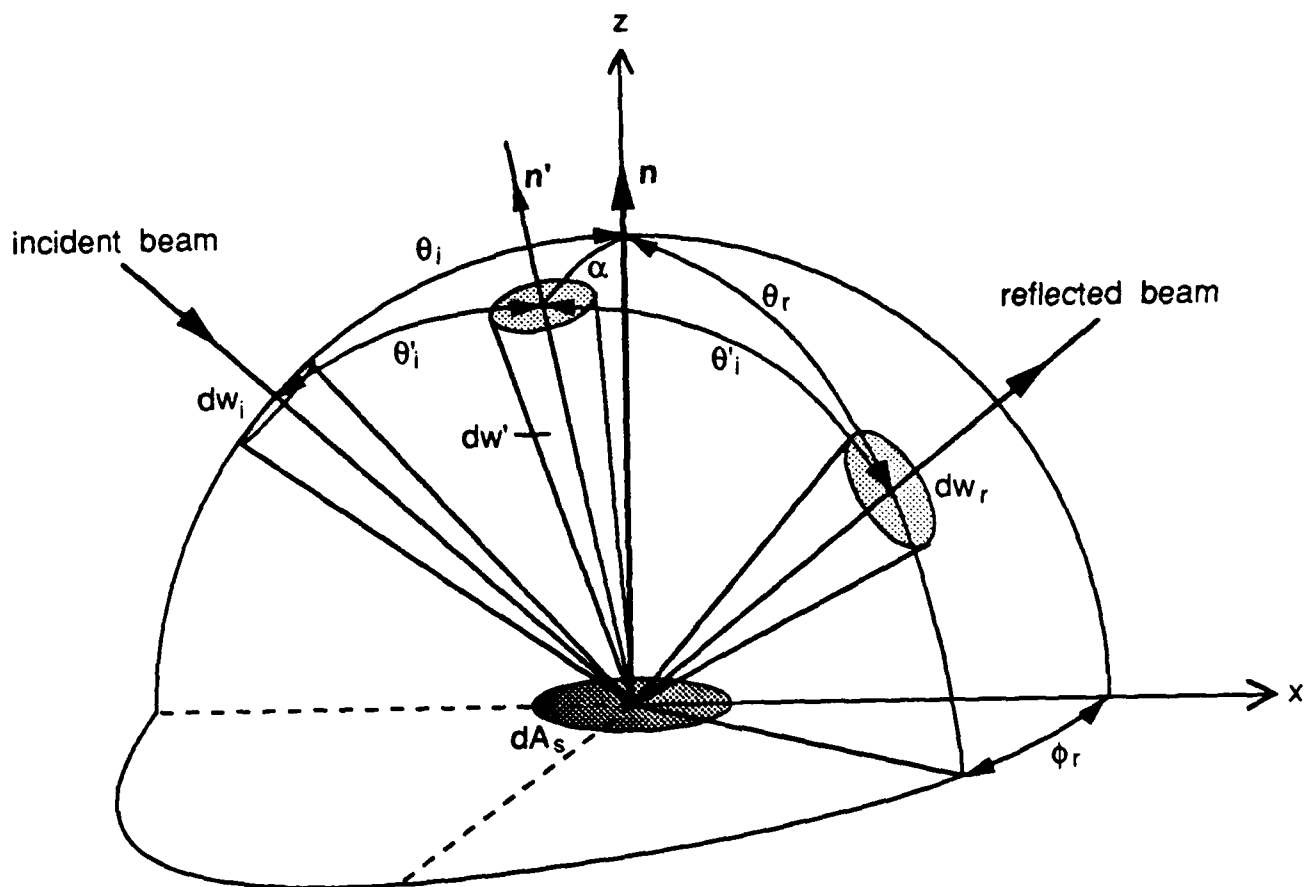
33

Figure 16: Coordinate system used to derive the Torrance-Sparrow model.

34

determine the electromagnetic field reflected in the specular direction by a planar surface when the incident wave is of parallel and perpendicular polarization, respectively. In this section, however, we are interested in the reflected flux, i.e. the energy flowing through a unit area. The reflection coefficients for energy reflectance may be determined from those for field reflectance as:

$$F'_{para}(\theta_i',\eta') = |F_{para}(\theta_i',\eta')|^2, \quad \text{and} \quad F'_{perp}(\theta_i',\eta') = |F_{perp}(\theta_i',\eta')|^2. \tag{62}$$

Let us assume that the polarization vector e_1 of the incident light wave lies outside the plane of incidence, and let h and v represent the magnitudes of the resolved components of e_1 in the parallel and perpendicular polarization planes, respectively. The Fresnel coefficient $F'(\theta_i',\eta')$ for the incident wave may be expressed as a linear combination of the Fresnel coefficients for parallel and perpendicular incident waves [25]:

$$F'(\theta_i',\eta') = h F'_{para}(\theta_i',\eta') + v F'_{perp}(\theta_i',\eta'), \tag{63}$$

where

$$h, v \geq 0 \text{ and } h + v = 1. \tag{64}$$

Torrance and Sparrow have also considered the masking and shadowing of one microfacet by adjacent facets. Adjacent facets may obstruct flux incident upon a given facet or the flux reflected by it. In order to compensate for these effects, the *geometrical attenuation factor*[7] $G(\theta_i,\theta_r,\phi_r)$ is introduced. The obstruction of incident or reflected light will depend on the angle of incidence and the angles of reflection. Each facet is assumed to be one side of a V-groove cavity, and light rays are assumed to be reflected only once. A detailed derivation of $G(\theta_i,\theta_r,\phi_r)$ is given in [30], and the final expression is found to be:

$$G(\theta_i,\theta_r,\phi_r) = min\left(1, \frac{2\cos\alpha\cos\theta_r}{\cos\theta_i'}, \frac{2\cos\alpha\cos\theta_i}{\cos\theta_i'}\right). \tag{65}$$

Taking the Fresnel reflection coefficient and the geometrical attenuation factor into consideration, the flux $d^2\Phi_r$ reflected into the solid angle $d\omega_r$ may be determined from the flux $d^2\Phi_i$ incident on the reflecting facets as:

$$d^2\Phi_r = F'(\theta_i',\eta') G(\theta_i,\theta_r,\phi_r) d^2\Phi_i. \tag{66}$$

The radiance L_r of the surface dA_s in the direction (θ_r,ϕ_r) is defined as:

$$L_r = \frac{d^2\Phi_r}{d\omega_r dA_s \cos\theta_r}. \tag{67}$$

---

[7]This factor plays the role of the shadowing function S mentioned in the previous section.

35

Using equations 61 and 66, equation 67 may be written as:

$$L_r = \frac{F'(\theta_i', \eta') \, G(\theta_i, \theta_r, \phi_r) \, L_i \, d\omega_i \, (a_f p_\alpha(\alpha) \, d\omega' \, dA_s) \cos\theta_i'}{d\omega_r \, dA_s \, \cos\theta_r} . \tag{68}$$

Earlier we stated that only facets with normals that lie within the solid angle $d\omega'$ are capable of reflecting light into the solid angle $d\omega_r$. Therefore, $d\omega'$ and $d\omega_r$ are related to one another. Though Torrance and Sparrow have only used this relationship and have not
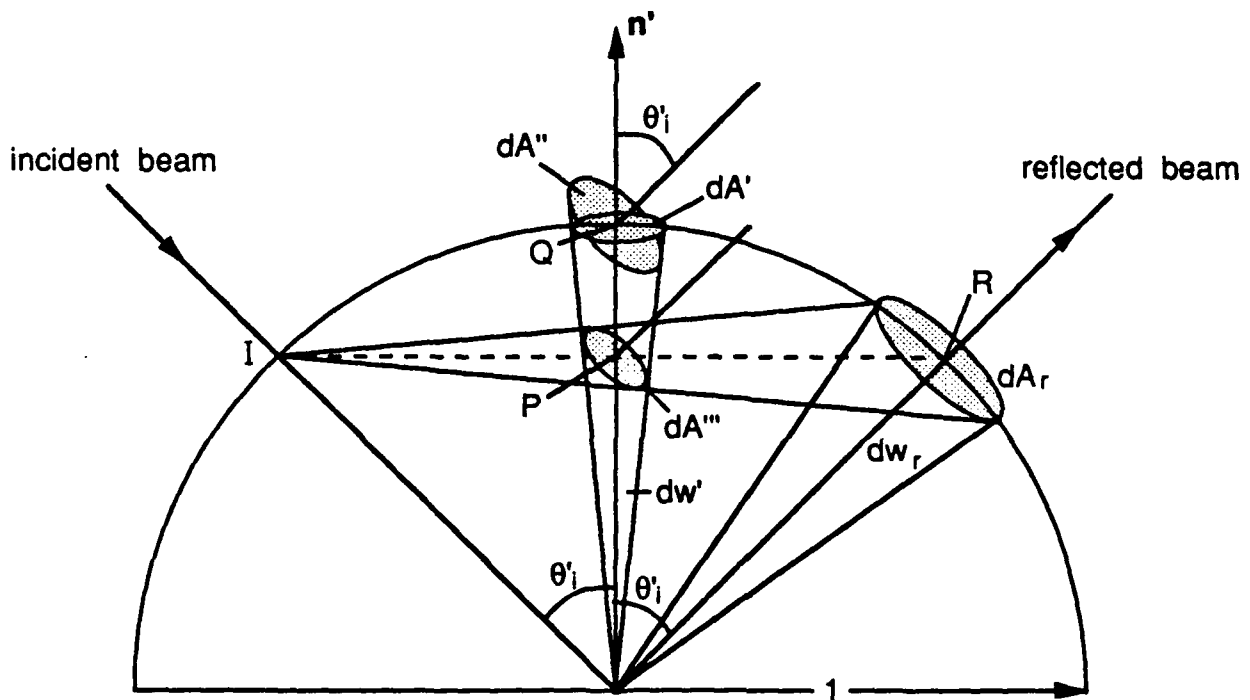
Figure 17: The source-viewer plane, illustrated to establish the relationship between $d\omega'$ and $d\omega_r$.

derived it, we feel that it is a very important one and deserves at least an informal proof. To this end, let us consider the plane shown in Figure 17, which includes the incident and reflected beams. We will assume all incident rays of light are parallel. This assumption is valid when the source is at a large distance from the surface. We see that the areas dA_r and dA''' subtend the same solid angle from the point I, and that $IR = 2IP$. Therefore, we can relate the two areas as $dA''' = dA_r/4$. Similarly, we see that dA'' and dA''' subtend the same solid angle $d\omega'$ from the point O. Noting that $OP = \cos\theta_i'$, we can relate the two areas as

36

$dA'' = dA'''/cos^2\theta_i'$. Further, the area dA' is a projection of the area dA'' onto the surface of the unit sphere, i.e. $dA' = dA''cos\theta_i$. Using the above relations, we can relate dA' to dA_r: $dA' = dA_r/4cos\theta_i'$. Since $dw' = dA'$ and $dw_r = dA_r$ (areas on the unit spheres), we have:

$$dw' = \frac{dw_r}{4\,cos\theta_i'} \quad . \tag{69}$$

Hence, for a given dw_r, the shape and size of the corresponding dw' is dependent on the local angle of incidence θ_i', which is in turn dependent on the angle of incidence θ_i and the angles of reflectance (θ_r, ϕ_r) (equation 59). Note that for a perfectly smooth surface, the parallel incident rays will be reflected in a single direction (the specular direction) and will not be scattered into a cone as shown in Figure 17. Therefore, for this limiting case, the above relationship between dw' and dw_r will not be valid.

Substituting equations 58 and 69 into equation 68, we obtain:

$$L_r = \kappa_{spec} \frac{L_i\,dw_i}{cos\theta_r} e^{-\frac{\alpha^2}{2\sigma_\alpha^2}} \quad , \tag{70}$$

where

$$\kappa_{spec} = \frac{c\,a_f F'(\theta_i', \eta')\,G(\theta_i, \theta_r, \phi_r)}{4} \quad . \tag{71}$$

Note the similarity between the above equation and the expression for the specular lobe predicted by the Beckmann-Spizzichino model (equation 49). Thus, the Torrance-Sparrow specular reflection model describes only the lobe component of specular reflection; there is no term in the above equation that represents the spike component of specular reflection. The radiance is determined only by the roughness parameter σ_α, and unlike the Beckmann-Spizzichino model, there is no dependence on the wavelength λ of incident light. However, from the physical optics model we have seen that the spike component is significant only when $\sigma_h/\lambda < 1.5$. Torrance and Sparrow have clearly stated that their model is only valid when $\sigma_h/\lambda \gg 1.0$. Therefore, this model must not be used to predict or interpret reflection from very smooth surfaces, i.e. when $\sigma_h/\lambda \ll 1.0$. To make their model more generic, Torrance and Sparrow have appended the Lambertian model to their specular model to account for diffuse reflection that may result from multiple reflections or internal scattering. Thus, for an angle of incidence θ_i, the radiance in the direction (θ_r, ϕ_r) of a rough surface whose facet slopes are normally distributed with standard deviation σ_α may be expressed as:

$$L_r = \kappa_{diff}\,max[\,0\,, (L_i\,dw_i\,cos\theta_i)\,] + \kappa_{spec} \frac{L_i\,dw_i}{cos\theta_r} e^{-\frac{\alpha^2}{2\sigma_\alpha^2}} \quad , \tag{72}$$

where κ_{diff} and κ_{spec} determine the fractions of incident energy that are reflected as components of the diffuse and specular lobes, respectively. From the radiance and irradiance, the BRDF

of the surface may be obtained as $f_r = L_r/I_s$. Once again, we will summarize the assumptions we have made during the derivation of this model and discuss the restrictions imposed by these assumptions.

4.2.3 Assumptions and Related Comments

- The surface is modeled as a collection of planar micro-facets, and the facet slopes are normally distributed. Other distributions, however, may be used to describe the facet slopes. For example, if the surface height is assumed to be normally distributed with standard deviation σ_h and correlation distance T, the slope distribution may be determined from the height distribution as [1]:

$$ p_\alpha(\alpha) = \frac{T}{2\,\sigma_h\,\sqrt{\pi}\,cos^2\alpha}\,\exp\left(\frac{tan^2\alpha}{2\,\sigma_h/T}\right)^2 . \qquad (73) $$

- The size of the planar facets is much greater than the wavelength of incident light, i.e. $\sigma_h \gg \lambda$. Therefore, we can assume that the light rays are reflected by each facet in its specular direction only. Furthermore, $\sigma_h \gg \lambda$ implies that the spike component of reflection is negligible and that the model determines only the lobe component of reflection.

- The geometrical model takes the Fresnel reflection coefficient F' into account. Therefore, the polarization of incident light and the conductivity of the surface medium need not be constrained. As a result, the model is capable of predicting reflections from both conductors and dielectrics.

- Each facet comprises one side of a symmetric V-groove cavity. With this assumption, the shadowing and masking effects are compensated for by using the geometrical attenuation factor G.

- The source is assumed to be at a great distance from the surface, so that all light rays that are incident upon the surface area dA_s are nearly parallel to one another. This assumption simplifies the relationship between the solid angles $d\omega'$ and $d\omega_r$ (equation 69).

- The final model includes the Lambertian model to account for diffuse reflection mechanisms such as multiple reflection and internal scattering.

4.2.4 Radiance Diagrams

Torrance and Sparrow have evaluated the performance of their model by plotting the ratio of the BRDF in a given direction to the BRDF in the specular direction. The normalized

38

BRDF distributions predicted by the model for a dielectric (MgO) and a conductor (Al) were found to fit the experimental data very well. We feel that plots of the normalized BRDF could lead to misinterpretation of the reflectance characteristics, however. Since image irradiance is proportional to surface radiance, we once again choose to plot absolute radiance diagrams. Since our intention is to compare the Torrance-Sparrow model with the Beckmann-Spizzichino model, we will neglect the Lambertian component of the Torrance-Sparrow model. Further, since the Torrance-Sparrow model is valid only when $\sigma_h \gg \lambda$, we will only compare it with the Beckmann-Spizzichino model for rough surfaces given by equation 49.
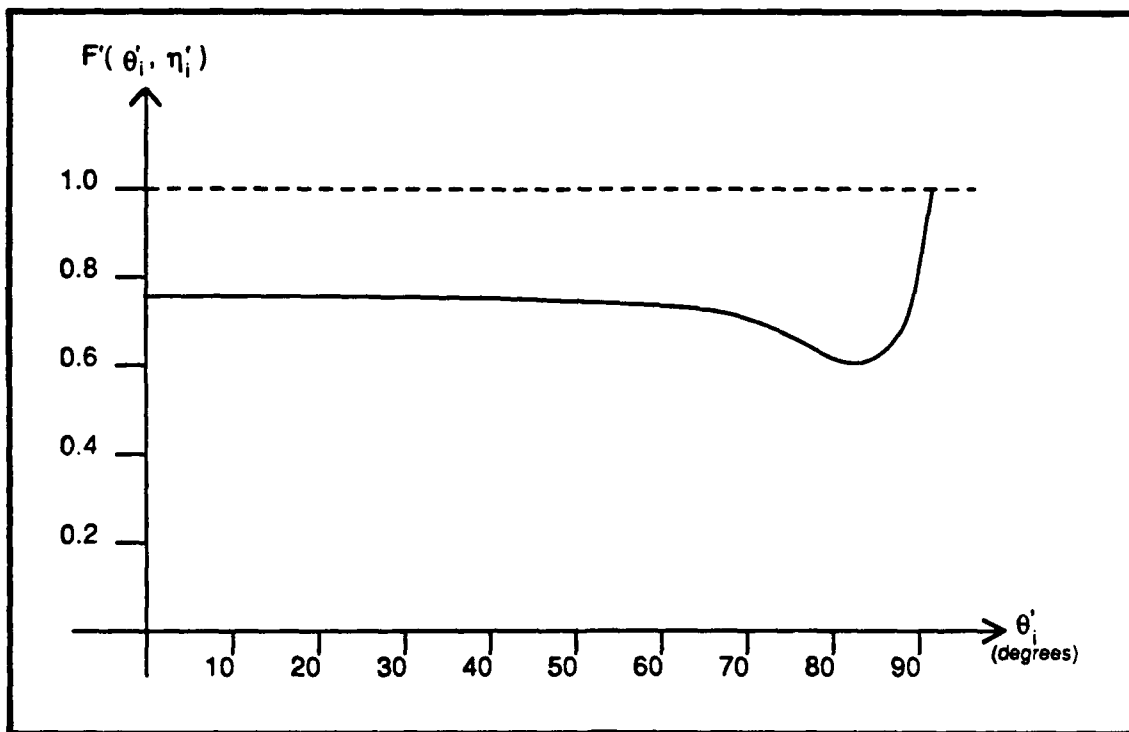
Figure 18: Typical plot of the Fresnel reflection coefficient as a function of the local incidence angle.

Consider the Fresnel coefficient $F'(\theta_i', \eta')$ and the geometrical attenuation factor $G(\theta_i, \theta_r, \phi_r)$ in equation 71. A typical plot of $F'(\theta_i', \eta')$ as a function of θ_i' is shown in Figure 18. For metals and many other surfaces, it is observed [20] that F' has a nearly constant behavior until the local angle of incidence θ_i' approaches 90 degrees. Therefore, we will assume that F' is constant with respect to θ_i and θ_r. Figure 19 shows $G(\theta_i, \theta_r, 0)$ plotted as a function of θ_r, for different values of θ_i. We see that, for angles of incidence not near

39

the grazing angle, G equals unity over an appreciable range of θ_r. In the following radiance diagrams, we will see that it is within these ranges of θ_r that the surface radiance attains maximum values. Therefore, we assume that $G = 1$ for all values of θ_i and θ_r. With the above two assumptions, we see that κ_{spec} is constant for all values of θ_i and θ_r.
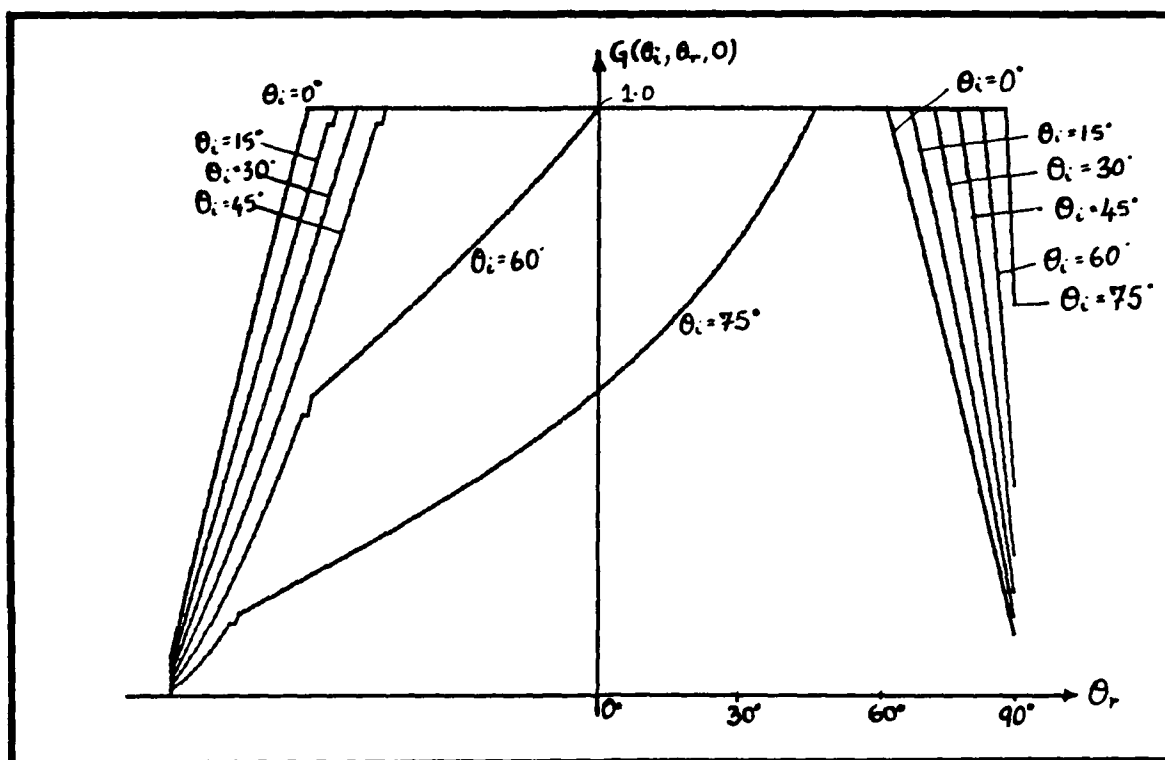

Figure 19: Geometrical attenuation function plotted as a function of the viewing angle, for different values of the incidence angle.

Figure 20 shows radiance diagrams for different values of the surface roughness parameter σ_α. Very small values of σ_α correspond to smooth surfaces, and for these values the specular lobes are similar in appearance to the specular spikes shown in Figure 11a. If the normalized BRDF is plotted rather than the absolute radiance, the lobe peaks will have constant values for all angles of incidence, and the resulting plot will appear exactly like the radiance diagram shown in Figure 11a. It is important to note that Figure 20a shows the specular lobes for a smooth surface and not the specular spikes. Therefore, the Torrance-Sparrow model is capable of predicting the specular lobe for smooth surfaces. However, for smooth surfaces, σ_h is comparable to λ, and the spike component is generally much stronger than the lobe component.
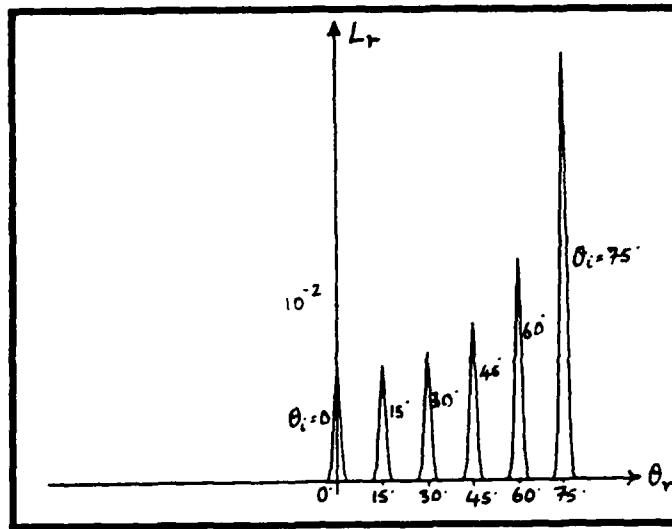
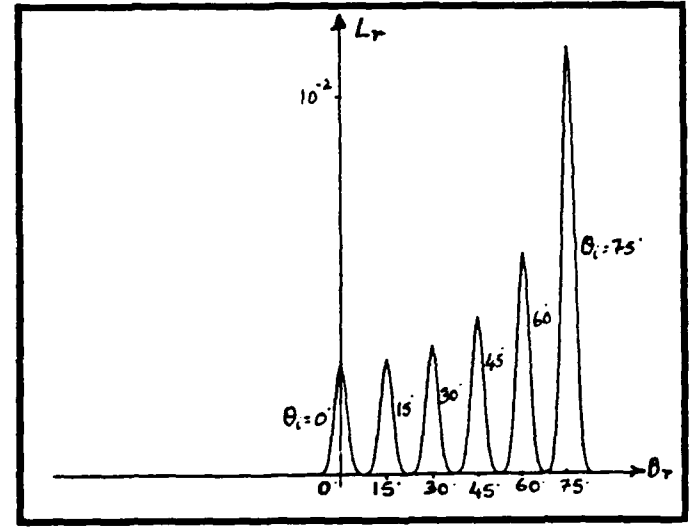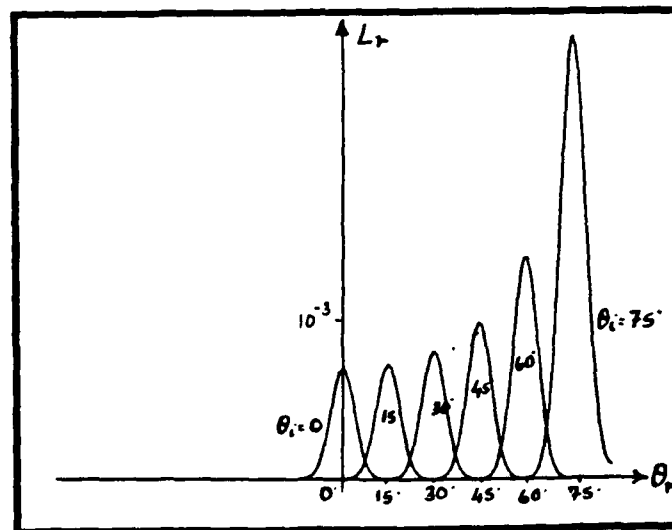We see from Figure 20 that the peak value of the specular lobe increases in magnitude
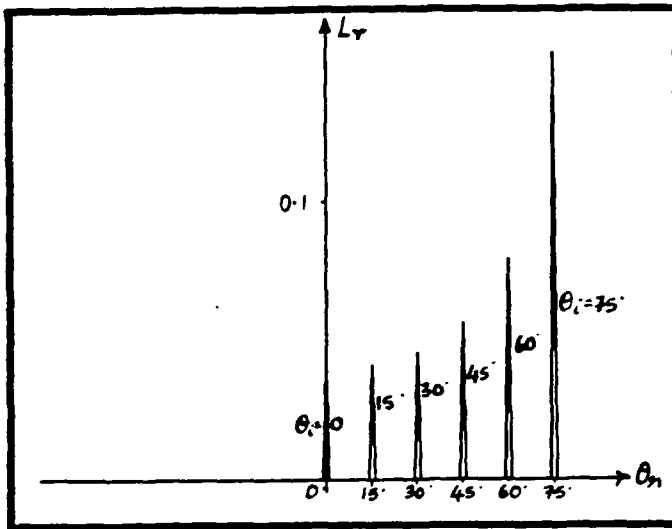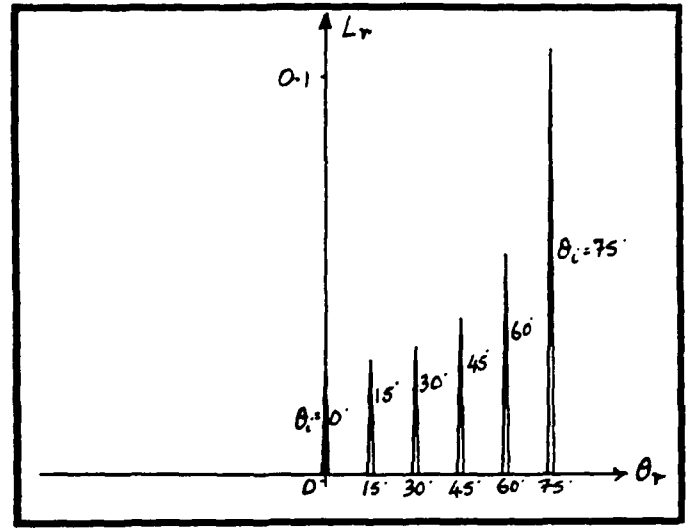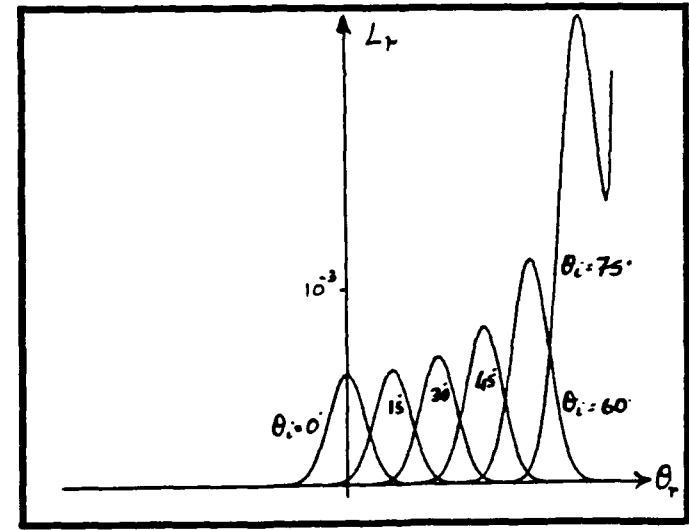
40

Figure 20: Radiance diagrams predicted by the Torrance-Sparrow model for different values of σ_α.
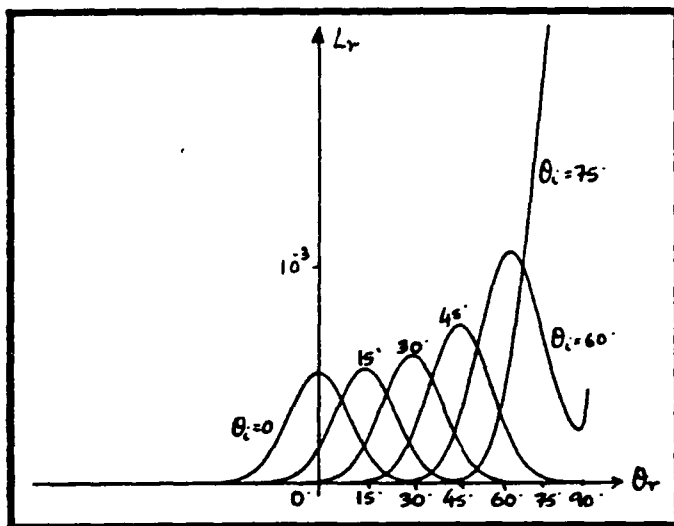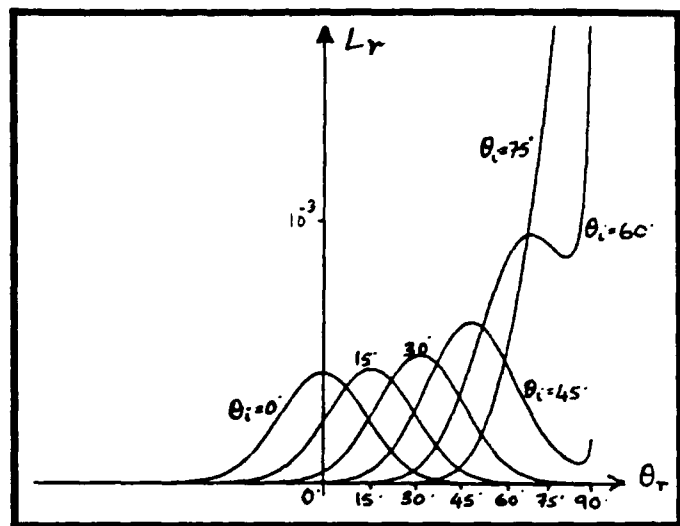
41
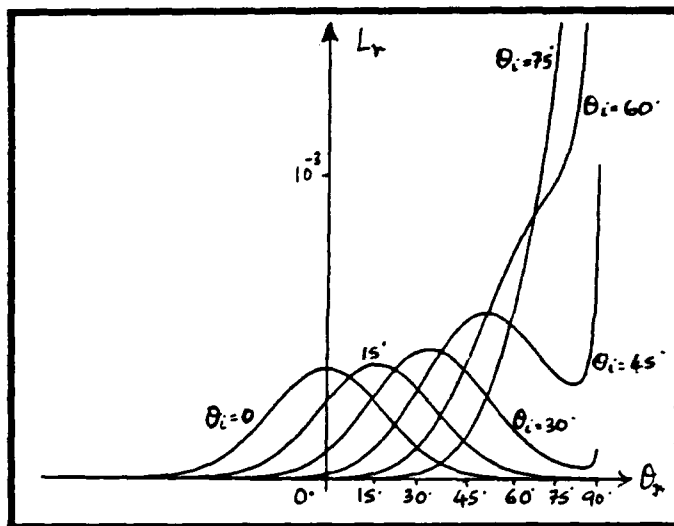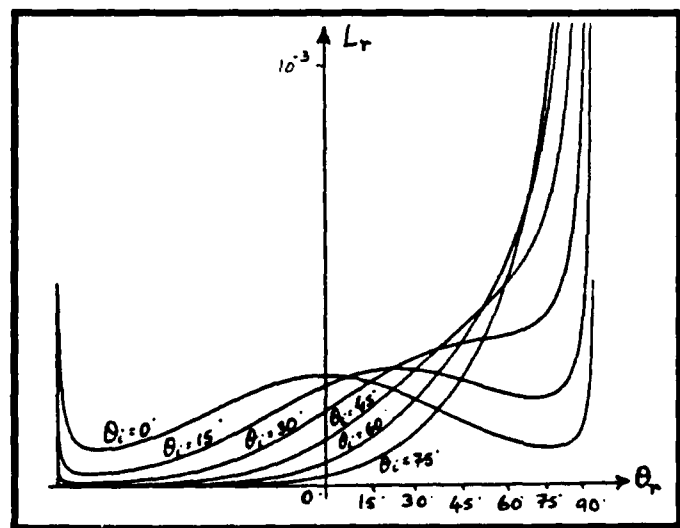
Figure 21: Radiance diagrams predicted by the Torrance-Sparrow model for different values of σ_α.

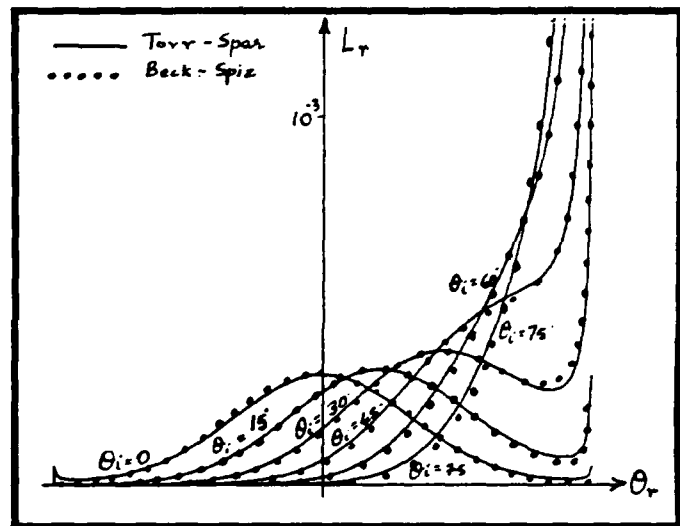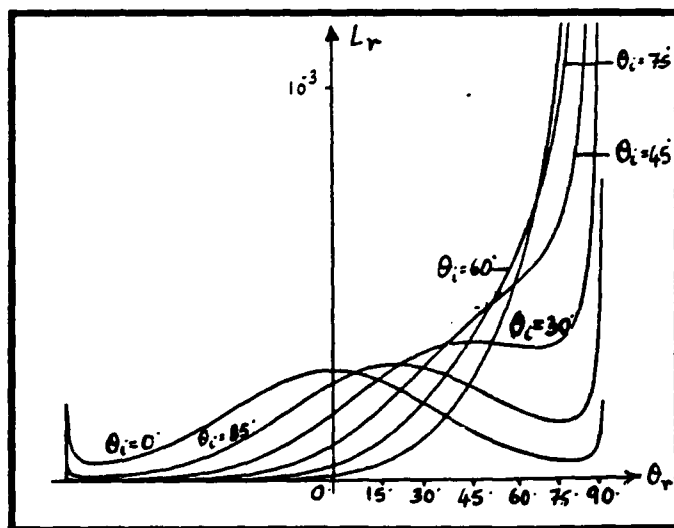with the angle of incidence θ_i. As in the case of the physical optics model, this effect results from the term $1/cos\theta_r$ (equation 70). It is also clear that the width of the lobe increases with the roughness parameter σ_α. In fact, for relatively small values of σ_α, the lobe may be approximated by a Gaussian function that is symmetric with respect to the specular direction. However, for higher values of σ_α (Figure 21), the lobe peak occurs at reflection angles greater than the specular angle. As with the physical optics model, these off-specular peaks result from the term $1/cos\theta_r$ (equation 70). For large values of θ_i and near-grazing values of θ_r, the radiance values approach infinity. From Figure 19 we see that G approaches zero for near-grazing values of θ_r. Torrance and Sparrow have proved that G approaches zero at a faster rate than the rate at which the plotted radiance approaches infinity. Hence, in practice, the surface radiance equals zero when $\theta_r = 90$ degrees. In Figure 21d, we have compared the radiance diagrams predicted by the Torrance-Sparrow model and the Beckmann-Spizzichino model. Though the two models were developed using different approaches and different surface models, we see that the resemblance between the two radiance diagrams is remarkable. In the following section, we relate the roughness parameters of the two models.

5 Observations

5.1 Primary Reflection Components

From the physical and geometrical optics reflection models, we see that surface radiance may be decomposed into three primary reflection components, namely, the diffuse lobe, specular lobe, and specular spike. Polar plots of these three components are illustrated in Figure 22. The sum of the three lobe components determines the surface radiance detected by the viewer for a fixed position of the source. The diffuse lobe is represented by the Lambertian model, and is constant with respect to the viewing direction. The specular lobe tends to be distributed around the specular direction, and has off-specular peaks for relatively large values of surface roughness. The specular spike is concentrated in a small region around the specular direction. The strengths of the specular lobe and specular spike components are related to one another. For a smooth surface, the specular spike component is many orders of magnitude greater than the specular lobe component. As the surface roughness increases, the spike component shrinks rapidly, and the specular lobe begins to dominate. We have seen from the radiance diagrams for the physical optics models that, for a given wavelength of incident light, the spike and lobe components are comparable to one another only for a small range of roughness values.

Owing to its simplicity and its conformity with experimental data [30], the specular component of the Torrance-Sparrow model may be used to approximate the specular lobe component. However, this model does not have a spike component, so the spike component
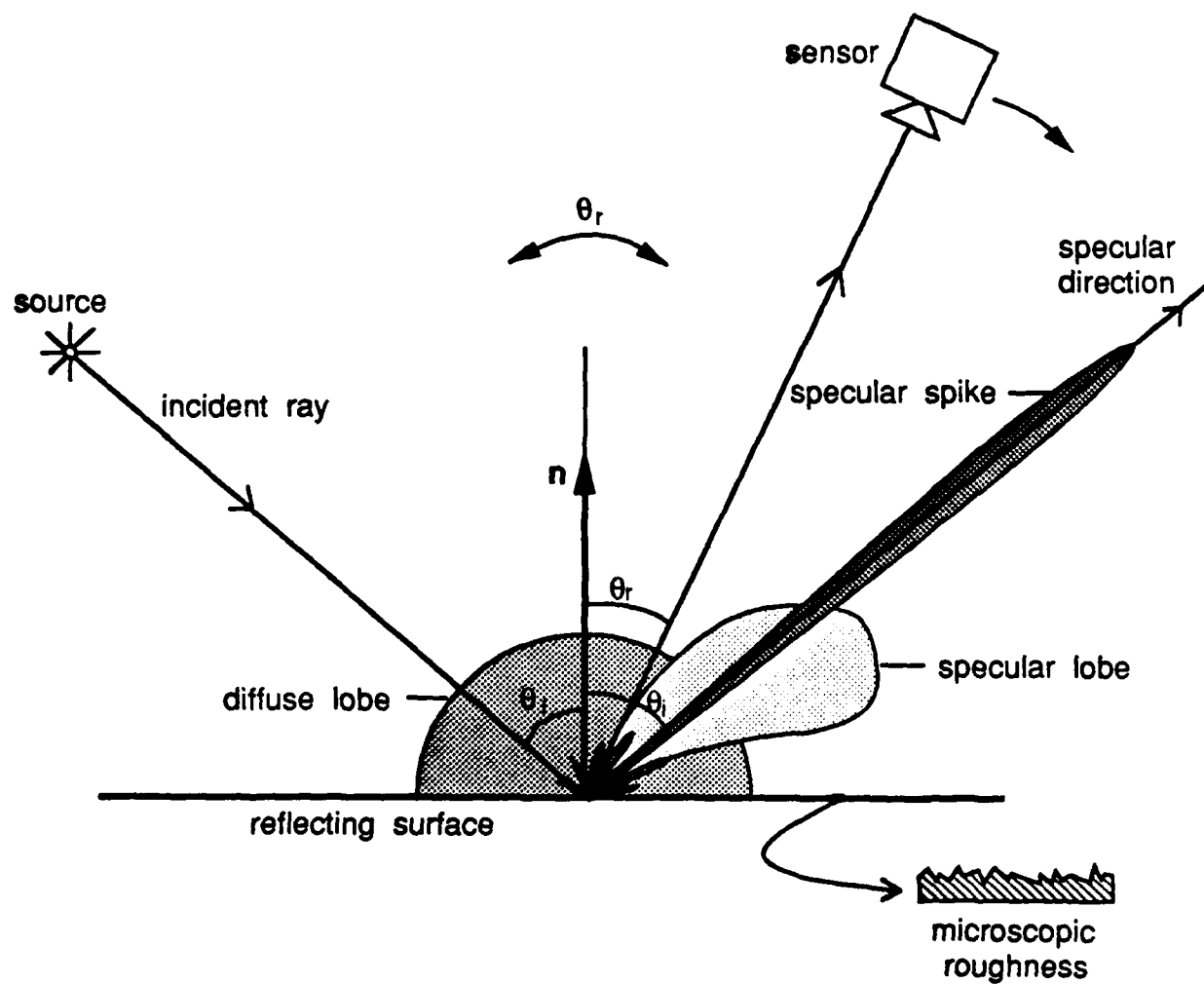
Figure 22: Polar plots of the three reflection components as functions of the viewing angle for a fixed source direction.

of the Beckmann-Spizzichino model may be used. We see from equation 47 that the shape of the spike component is determine by the term ρ_o. Since ρ_o is a very sharp function of θ_i and θ_r, we can approximate ρ_o by a Gaussian function with low standard deviation or a double-delta function. Using the above approximations, the image irradiance equation, for fixed source direction and varying sensor direction, may be written as a linear combination of the three reflection components:

$$I_{im} = C_{dl} + \frac{C_{sl}}{cos\theta_r} exp\left(-\frac{\alpha^2}{2\sigma_\alpha^2}\right) + C_{ss}\,\delta\,(\theta_i - \theta_r)\,\delta\,(\phi_r)\,, \tag{74}$$

where, the constants C_{dl}, C_{sl}, and C_{ss} represent the strengths of the diffuse lobe, specular lobe, and specular spike components, respectively.

5.2 Moving Source and Fixed View

In all the radiance diagrams we have presented so far, surface radiance was plotted as a function of viewing direction θ_r, for fixed values of the incidence angle θ_i. In shape extraction techniques such as photometric stereo, structured highlight, and photometric sampling, however, images of the observed object are obtained by varying the source direction while keeping the viewing direction constant. Note that when the viewing direction is fixed, the term $1/cos\theta_r$ in the specular component of the Torrance-Sparrow model (equation 72) is constant, and the shape of the specular lobe is dependent solely on the term

$$exp\left(-\frac{\alpha^2}{2\sigma_\alpha^2}\right)\,. \tag{75}$$

Since $\alpha = 0$ when $\theta_r = \theta_i$, the specular lobe is found to be symmetric with respect to the specular direction. A similar analysis is applicable to the physical optics model for rough surfaces (equation 49). The only term that is significantly affected by variations in θ_i is the term $e^{-v_{xy}^2 T^2 / 4v_z^2 \sigma_h^2}$. Further, it can be shown [1] that

$$tan\,\alpha = \frac{v_{xy}}{v_z}\,, \tag{76}$$

where, as with the slope distribution model, α is the angle between the bisector of the incident and viewing directions and the surface normal vector $\mathbf{n}$. Let us assume that $tan\,\alpha_o = 2\,\sigma_h/T$. Then, we can write:

$$exp\left(-\frac{v_{xy}^2 T^2}{4\,v_z^2\,\sigma_h^2}\right) = exp\left(-\frac{tan^2\,\alpha}{tan^2\,\alpha_o}\right)\,. \tag{77}$$

45

Many rough surfaces are gently varying, and the slopes (α) of most facets are small. Therefore, we may approximate the tangents in equation 77 by their arguments, obtaining:

$$exp\left(-\frac{v_{xy}^2 T^2}{4 v_z^2 \sigma_h^2}\right) = exp\left(-\frac{\alpha^2}{2\left(\alpha_o/\sqrt{2}\right)^2}\right) . \tag{78}$$

From equations 78 and 75, we see that the roughness parameters of the Torrance-Sparrow model and the Beckmann-Spizzichino model may be related as:

$$\sigma_\alpha = \frac{\alpha_o}{\sqrt{2}} = \frac{1}{\sqrt{2}} tan^{-1} \frac{2\sigma_h}{T} . \tag{79}$$

Figure 23 shows radiance diagrams plotted for surfaces with different roughness values using the Beckmann-Spizzichino model (left column) and the Torrance-Sparrow model (right column). Here again, only the specular lobe component is considered. Note that these radiance diagrams differ from all of the previous ones in that radiance is plotted as a function of the source angle θ_i for fixed values of the viewing angle θ_r, rather than vice-versa. Once again we assume that $\phi_r = 0$, the geometrical attenuation factor equals unity, and the Fresnel reflection coefficient is constant. For each σ_h/T ratio in the left column, we have used equation 79 to find σ_α for the corresponding diagram in the right column. Three important observations can be made from these radiance diagrams:

- When the source direction, viewer direction, and surface normal are coplanar, the radiance curves can be represented by Gaussian functions. This statement can be proved analytically by setting $\phi_r = 0$ in the specular lobe component of both models.

- The peak for each radiance curve is observed at the specular angle, i.e. $\theta_i = \theta_r$. Varying source direction, rather than viewing direction, prevents off-specular peaks from occurring. In addition, the radiance value exhibits reflection symmetry with respect to the viewer-normal plane.

- The radiance diagrams predicted by the physical optics and the geometrical optics models resemble each other very strongly. Therefore, even though the two models use two different surface modeling parameters (height and slope, respectively), equation 79 does very well in relating the physical roughness parameters of the two models.

We can further illustrate the difference between varying source direction and varying viewer direction by introducing a new representation of the reflection components. Figure 24 shows polar plots of the diffuse lobe, specular lobe, and specular spike. This time, however, the magnitudes of the three components of the radiance value in the viewing direction are determined by intersections made by the lobes with the line joining the source and the
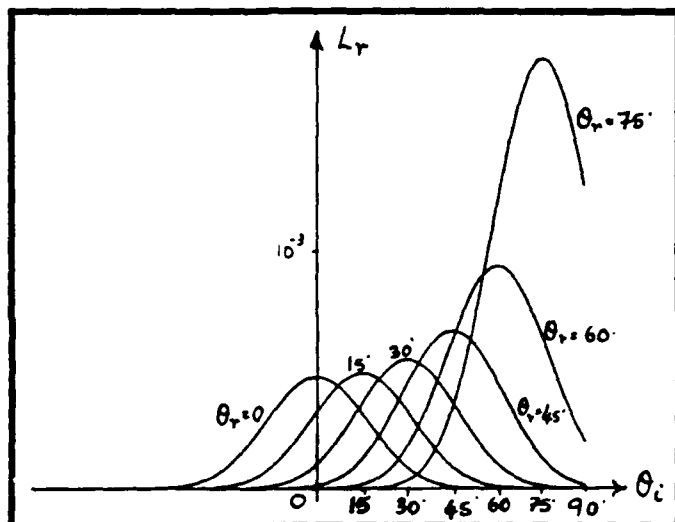
46

Beckmann - Spizzichino
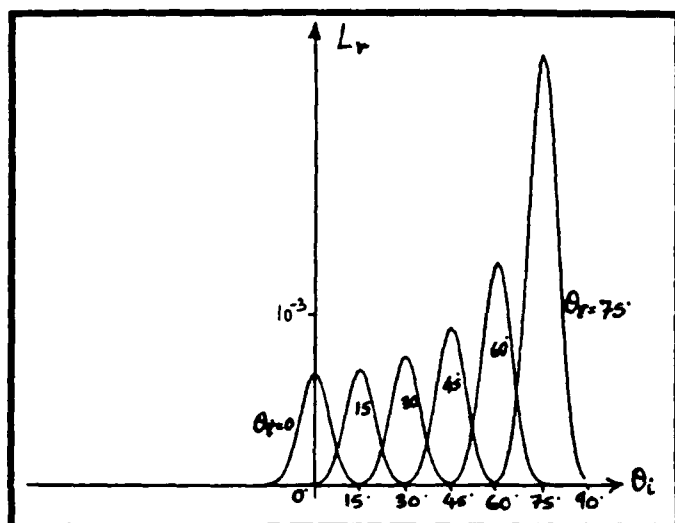
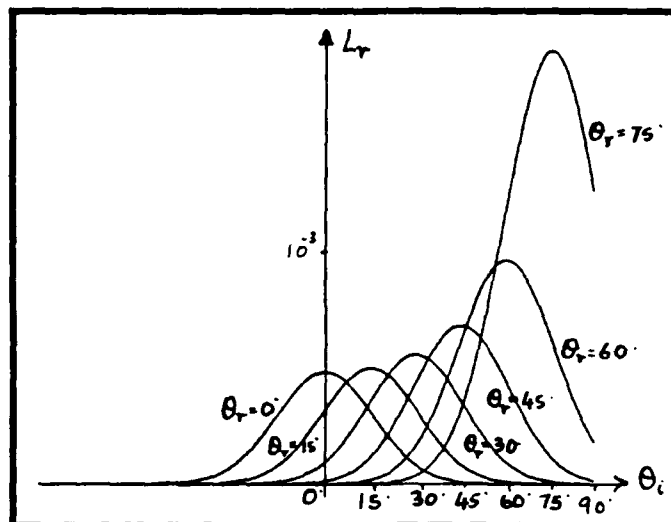## Torrance - Sparrow

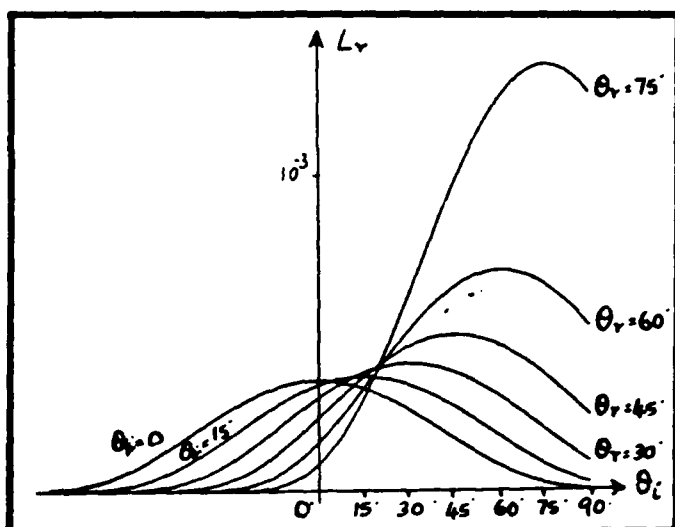(a) $\sigma_h = 0.003$, $T = 0.01$, $\lambda = 0.001$
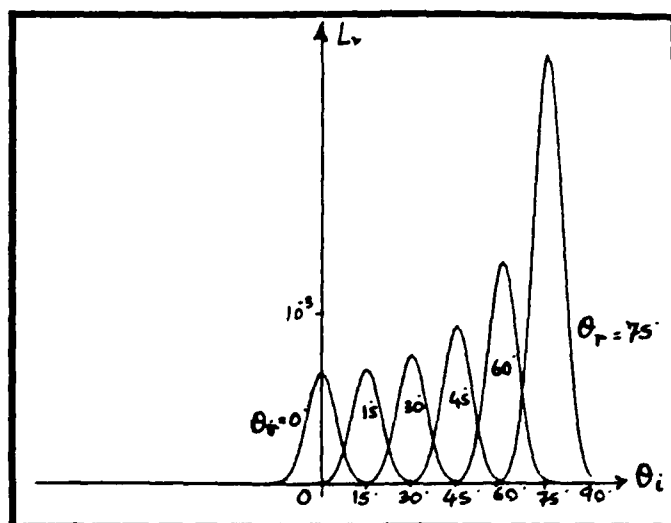
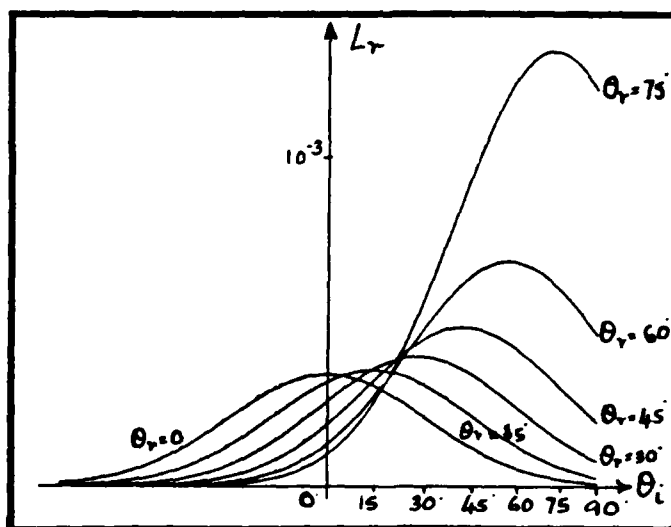(b) $\sigma_\alpha = 2.428$

(c) $\sigma_h = 0.001$, $T = 0.01$, $\lambda = 0.001$

(d) $\sigma_\alpha = 7.99$

(e) $\sigma_h = 0.002$, $T = 0.01$, $\lambda = 0.001$

(f) $\sigma_\alpha = 15.416$

Figure 23: Radiance diagrams predicted by the Beckmann-Spizzichino model and the Torrance-Sparrow model. In these diagrams, radiance is plotted as a function of θ_i for fixed values of θ_r.
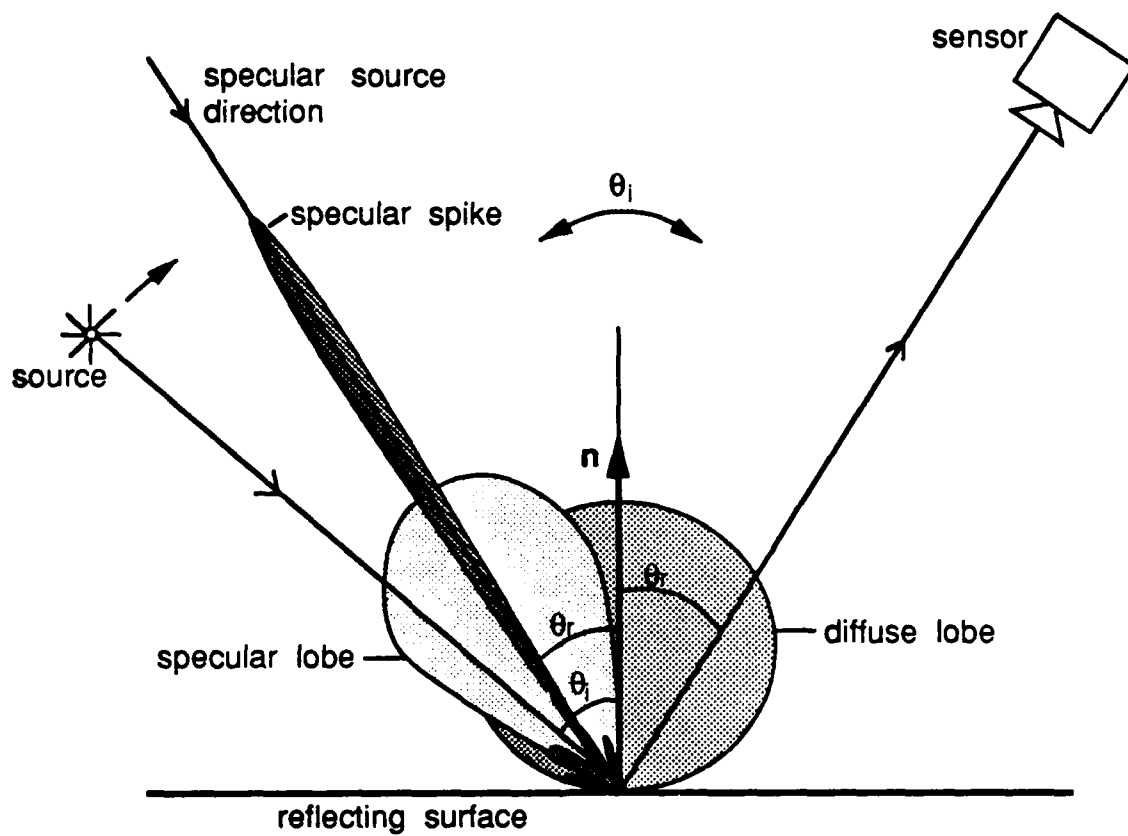
47

Figure 24: Polar plots of the three reflection components as functions of the source angle for a fixed viewing direction.

origin. In this case, the diffuse component varies with the position of the source, since it is proportional to the surface irradiance. Note that the specular lobe is symmetric with respect to the source specular angle $\theta_i = \theta_r$, and the spike is concentrated around the same angle. From the above observations, the image irradiance equation, for fixed sensor direction and varying source direction, may be written:

$$I_{im} = K_{dl} \cos\theta_i + K_{sl} \exp \left(-\frac{\alpha^2}{2\sigma_\alpha^2} \right) + K_{ss} \delta (\theta_i - \theta_r) \delta (\phi_r) , \qquad (80)$$

where the constants K_{dl}, K_{sl}, and K_{ss} represent the strengths of the diffuse lobe, specular lobe, and specular spike components, respectively. Note that the ratio K_{sl}/K_{ss} is dependent on the surface roughness and the angles of incidence and reflection. Seldom are K_{sl} and K_{ss} comparable to one another. In most instances, one of the two specular components is significant, while the other is negligible.

6 Concluding Remarks

- We propose a reflection model with three primary components: the diffuse lobe component, the specular lobe component, and the specular spike component.

- The Lambertian model may be used to represent the diffuse lobe component. This model has been used extensively to test shape-from-shading and photometric stereo techniques, and the results have indicated that it performs reasonably well. More accurate models [14] [21] may be used at the cost of functional complexity.

- The Beckmann-Spizzichino physical optics model predicts both the specular lobe and spike components. For a very smooth surface ($\sigma_h \ll \lambda$), the spike component dominates and the surface behaves like a mirror. As the roughness increases, however, the spike component shrinks rapidly, and the lobe component begins to dominate. The two components are simultaneously significant for only a small range of roughness values.

- A sharp specular component may result from the specular spike component when the surface is smooth ($\sigma_h/\lambda < 1.5$), and/or from the specular lobe component when the surface is gently undulating ($\sigma_h/T < 0.02$).

- The Torrance-Sparrow geometrical optics model provides a good approximation to the specular lobe component of the Beckmann-Spizzichino model. Both models are successful in predicting off-specular peaks in the specular lobe component. Owing to its simpler mathematical form, the Torrance-Sparrow model may be used to represent the specular lobe component.

49

- The Torrance-Sparrow model is not capable of describing the mirror-like behavior of smooth surfaces, and it should not be used to represent the specular spike component as it would produce erroneous results.

- The specular lobes of both Torrance-Sparrow, and Beckmann-Spizzichino models tend to have specular peaks, rather than off-specular peaks, when the viewing direction is fixed and the source direction is varied.

- Though the two models were derived using different surface modeling approaches, their surface roughness parameters may be related to one another by comparing the equations that describe their specular lobe components.

Acknowledgements

References

[1] P. Beckmann and A. Spizzichino, *The Scattering of Electromagnetic Waves from Rough Surfaces,* Pergamon Press, 1963.

[2] E. V. Bohn, *Introduction to Electromagnetic Fields and Waves,* Addison-Wesley Publishing Co., 1967.

[3] S. Chandrashekar, *Radiative Transfer,* Dover Publications Inc., 1960.

[4] E. N. Coleman and R. Jain, *Obtaining 3-dimensional shape of textured and specular surface using four-source photometry,* Computer Graphics and Image Processing, Vol. 18, No. 4, pp. 309-328, April, 1982.

[5] R. L. Cook and K. E. Torrance, *A Reflectance Model for Computer Graphics,* Proceedings, Siggraph, Vol. 15, No. 3, pp. 307-316.

[6] G. Healey and T. O. Binford, *Local Shape from Specularity,* Proc. Image Understanding Workshop, Vol. 2, pp. 874-887, February, 1987.

[7] B. K. P. Horn, *Hill Shading and the Reflectance Map,* Proc. of the IEEE, Vol. 69, No. 1, pp. 14-47, January 1981.

[8] B. K. P. Horn and R. W. Sjoberg, *Calculating the reflectance map,* Applied Optics, Vol. 18, No. 11, pp. 1770-1779, June 1979.

[9] B. K. P. Horn, *Image intensity understanding,* Artificial Intelligence, Vol. 8, No. 2, 1977.

[10] B. K. P. Horn, *Robot Vision,* MIT Press, 1986.

[11] A. F. Houchens and R. G. Hering, *Bidirectional Reflectance of Rough Metal Surfaces,* Thermophysics of Spacecraft and Planetary Bodies, G. B. Heller, Eds. Academic Press, 1967.

[12] K. Ikeuchi, *Determining surface orientations of specular surfaces by using the photometric stereo method*, IEEE Trans. on Pattern Analysis and Machine Intelligence, Vol. 3, No. 6, pp. 661-669, November, 1981.

[13] G. J. Klinker, S. A. Shafer, and T. Kanade, *The Measurement of Highlights in Color Images*, International Journal of Computer Vision, Vol. 2, No. 1, Spring, 1988.

[14] P. Kubelka and F. Munk, *Ein Beitrag sur Optik der Farbanstriche*, Z. tech. Physik, Vol. 12, 593, 1931.

[15] J. H. Lambert, *Photometria sive de mensura de gratibus luminis, colorum et umbrae*, Eberhard Klett, Augsburg, 1760.

[16] S. K. Nayar, K. Ikeuchi, T. Kanade, *Extracting Shape and Reflectance of Lambertian, Specular, and Hybrid Surfaces*, CMU-RI-TR-88-14, August, 1988.

[17] F. E. Nicodemus, J. C. Richmond, J. J. Hsia, I. W. Ginsberg, and T. Limperis, *Geometrical Considerations and Nomenclature for Reflectance*, NBS Monograph 160, National Bureau of Standards, October 1977.

[18] A. P. Pentland, *Local Shading Analysis*, IEEE Trans. on Pattern Analysis and Machine Intelligence, Vol. 6, No. 2, pp. 170-187, March, 1984.

[19] B. Phong, *Illumination for Computer Generated Pictures*, Communications of ACM, Vol. 18, pp. 311-317, 1975.

[20] *Physics Handbook*, American Institute of Physics Handbook, McGraw-Hill, 1972.

[21] J. Reichman, *Determination of Absorption and Scattering Coefficients for Nonhomogeneous Media. 1: Theory*, Applied Optics, Vol. 12, No. 8, pp. 1811-1815, August, 1973.

[22] J. Reichman, *Determination of Absorption and Scattering Coefficients for Nonhomogeneous Media. 1: Theory*, Applied Optics, Vol. 12, No. 8, pp. 1816-1823, August, 1973.

[23] W. A. Rense, *Polarization Studies of Light Diffusely Reflected from Ground and Etched Glass Surfaces*, Journal of Optical Society of America, Vol. 40, No. 1, pp. 55-59, January 1950.

[24] A. C. Sanderson, L. E. Weiss, and S. K. Nayar, *Structured Highlight Inspection of specular surfaces*, IEEE Trans. on Pattern Analysis and Machine Intelligence, Vol. 10, No. 1, pp. 44-55, January, 1988.

[25] R. Siegel and J. R. Howell, *Thermal Radiation Heat Transfer*, McGraw-Hill, 1972.

[26] W. M. Silver, *Determining Shape and Reflectance Using Multiple Images,* S. M. Thesis, Dept. of Electrical Engineering and Computer Science, MIT, Cambridge, Massachusetts, June, 1980.

[27] B. G. Smith, *Geometrical Shadowing of a Random Rough Surface,* IEEE Trans. Ant. and Propogation, Vol. 15, No. 5, pp. 668-671, Sept. 1967.

[28] E. Sparrow and R. Cess, *Radiation Heat Transfer,* McGraw-Hill, 1978.

[29] H. D. Tagare and Rui J. P. deFigueiredo, *A Framework for the Construction of General Reflectance Maps for Machine Vision,* Technical Report, Dept. of Elec. and Comp. Engg., Rice University.

[30] K. Torrance and E. Sparrow, *Theory for Off-Specular Reflection from Roughened Surfaces,* Journal of the Optical Society of America, No. 57, pp. 1105-1114, 1967.

[31] L. B. Wolff, *Spectral and Polarization Stereo Methods using a Single Light Source* Proc. Image Understanding Workshop, Vol. 2, pp. 810-820, February, 1987.

[32] R. J. Woodham, *Photometric stereo: A reflectance map technique for determining surface orientation from image intensity,* Proc. SPIE, Vol. 155, pp. 136-143, 1978.